



**NEUTRON SHIELDING EFFECTIVENESS OF
MULTIFUNCTIONAL COMPOSITE MATERIALS**

THESIS

Anthony D. Marchand, MAJ, USA

AFIT-ENP-13-M-25

**DEPARTMENT OF THE AIR FORCE
AIR UNIVERSITY**

AIR FORCE INSTITUTE OF TECHNOLOGY

Wright-Patterson Air Force Base, Ohio.

**DISTRIBUTION STATEMENT A.
APPROVED FOR PUBLIC RELEASE; DISTRIBUTION UNLIMITED**

The views expressed in this thesis are those of the author and do not reflect the official policy or position of the United States Air Force, Department of Defense, or United States Government. This material is declared a work of the U.S. Government and is not subject to copyright protection in the United States.

AFIT-ENP-13-M-25

NEUTRON SHIELDING EFFECTIVENESS OF
MULTIFUNCTIONAL COMPOSITE MATERIALS

THESIS

Presented to the Faculty

Department of Engineering Physics

Graduate School of Engineering and Management

Air Force Institute of Technology

Air University

Air Education and Training Command

In Partial Fulfillment of the Requirements for the
Degree of Master of Science in Nuclear Engineering

Anthony D. Marchand, B.S.

MAJ, USA

March 2013

DISTRIBUTION STATEMENT A.
APPROVED FOR PUBLIC RELEASE; DISTRIBUTION UNLIMITED

NEUTRON SHIELDING EFFECTIVENESS OF
MULTIFUNCTIONAL COMPOSITE MATERIALS

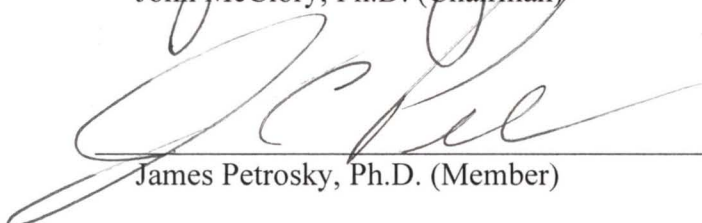
Anthony D Marchand, B.S.
MAJ, USA

Approved:



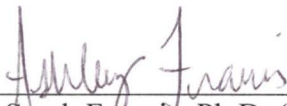
John McClory, Ph.D. (Chairman)

4 MAR 2013
Date



James Petrosky, Ph.D. (Member)

4 MAR 13
Date



Sarah Francis, Ph.D. (Member)

3/4/13
Date



Justin Clinton, Ph.D. (Member)

4 March 2013
Date

ABSTRACT

Composite materials offer a greater degree of flexibility in design and engineering of specialized space vehicle shielding applications compared to aluminum. A new design for shielding materials has been developed by including specific neutron absorbers and conductive materials into the composite structure. In this research, the neutron shielding capability of two types of custom-designed nanocomposite materials are compared to that of T6061 aluminum; simulations using a Monte Carlo Neutral-Particle code are used to complement and aid in the design of the materials and the experimental setup. Simulations predict the composite material with boron captures 1.72% of 2.45 MeV neutrons compared to the T6061 aluminum, which captures 0.01% of the neutrons. When normalizing the density of the composites to T6061 in the simulations, the composite material with boron transmits 88.67% of the neutrons, and the composite without boron transmits 66.44% of the neutrons. To verify the simulation results, experiments were conducted to measure the relative effectiveness of neutron shielding for three samples of varying thickness consisting of: aluminum, a composite without boron, and a composite with boron. One experiment used a tissue equivalent proportional counter (TEPC) using the Air Force Institute of Technology's (AFIT's) PuBe neutron source to measure the relative changes in the amount of recoil protons detected when different shielding materials were placed in front of the detector. The results showed that the composite without boron provided the best shielding from neutrons. A second experiment measured shielding effectiveness of the same samples from a PuBe neutron source using foil activation analysis of indium, zinc, and gold foils. The results

demonstrated that, after normalization, the composite without boron shielded fast neutrons more effectively than the other materials overall, but the sample with boron shielded thermal neutrons 60% better than aluminum. Overall, there is promise in this composite material, but the fast neutrons are not down-scattered sufficiently in the composite to allow absorption by the boron. In the future, developing more efficient ways to slow fast neutrons will allow the borated composite to become a better shielding material against neutrons.

Acknowledgments

I would like to express my sincere appreciation to my faculty advisor, Dr. John McClory, for his guidance and support throughout the course of this thesis. His insight and experience was certainly appreciated. I would also like to thank my sponsor, Max Alexander, from the Air Force Research Lab for helping me obtain the material for this thesis. I would also like to thank Jason Cezeaux from the Air Force Radiological Assessment Team for allowing me to sign out most of the experimental equipment for this thesis. I would like to thank Dr. Justin Clinton for all his teaching and aiding in experimental setup and procedures in this thesis. I would also like to thank Major Ben Kowash for all this modeling and experimental help provided for this thesis. I would like to thank Eric Taylor for all his assistance in Lab setup and maintaining the equipment. I would like to thank my proof readers: Colonel (Ret) Russ Furstnow, Marilyn Peterson, Major Maurice Wilson, and Dr. Ashley Francis.

Anthony D. Marchand

Table of Contents	Page
Abstract.....	v
Acknowledgments	vii
Table of Contents.....	viii
List of Figures	xi
List of Tables	xv
CHAPTER 1 INTRODUCTION	1
1.1 Background.....	1
1.2 Objective of Research	2
1.3 Paper Organization	4
CHAPTER 2 THEORY	5
2.1 Overview.....	5
2.2 Moderating Neutrons	5
2.3 Intensity of Neutrons through a Material.....	7
CHAPTER 3 MODELING.....	9
3.1 Introduction.....	9
3.2 Assumptions.....	9
3.3 Modeling Results and Analysis	13
3.4 Modeling Conclusion.....	20
CHAPTER 4 EXPERIMENT	21
4.1 Introduction.....	21
4.2 Foil Activation Experiment	21

4.3	Tissue Equivalent Proportional Counter Experiment	28
CHAPTER 5 EXPERIMENTAL RESULTS AND ANALYSIS.....		35
5.1	Tissue Equivalent Proportional Counter Experiment	35
5.1.1	Aluminum Shielding with TEPC	35
5.1.2	Sample X_{w0B} Shielding with TEPC	37
5.1.3	Sample X_{wB} Shielding with TEPC.....	38
5.1.4	TEPC versus One Layer of Shielding.....	40
5.1.5	TEPC versus Two Layers of Shielding.....	41
5.1.6	TEPC versus Three Layers of Shielding.....	42
5.1.7	Summary of TEPC Experiment	44
5.2	Foil Activation Experiment	47
5.2.1	Foil Activation with Indium Foils.....	48
5.2.2	Foil Activation with Zinc Foils.....	50
5.2.3	Foil Activation with Gold Foils	53
5.2.4	Summary of Foil Activation Experiment.....	55
CHAPTER 6 CONCLUSION		57
6.1	Summary of Findings.....	57
6.2	Future Work.....	60
APPENDIX A – Simulation Codes		61
APPENDIX B – Filling the LET Detector		63
APPENDIX C – TEPC		66
APPENDIX D – FOIL ACTIVATION		84

BIBLIOGRAPHY	87
--------------------	----

LIST OF FIGURES

	Page
Figure 1: Illustration of the model used in MCNP.	10
Figure 2: MCNP results that illustrates the accuracy of the simulation versus the amount of time to run a simulation	12
Figure 3: MCNP simulation for T6061 aluminum	13
Figure 4: MCNP simulation for sample X_{woB}	14
Figure 5: MCNP simulation for sample X_{wB}	15
Figure 6: Combination plot of all MCNP simulations.....	16
Figure 7: Total neutron cross section for boron and gadolinium from ENDF.....	18
Figure 8: Engineering limit combination plot.....	19
Figure 9: Total activity of sample X_{wB} , 16 hours following a 10 hour irradiation with a neutron flux of 1×10^8 neutrons/cm ² /sec.....	22
Figure 10: Total activity of sample X_{woB} , 16 hours following a 10 hour irradiation with a neutron flux of 1×10^8 neutrons/cm ² /sec.....	23
Figure 11: Total activity of T6061, 16 hours following a 10 hour irradiation with a neutron flux of 1×10^8 neutrons/cm ² /sec.....	23
Figure 12: PuBe neutron source spectrum	25
Figure 13: Experimental setup for foil activation using the PuBe source in building 470.	26
Figure 14: Recoil proton spectrum for ^{252}Cf	29
Figure 15: Setup of the TEPC with the gas filling system.....	30

Figure 16: Close-up view of the three layer shielding box.	32
Figure 17: Experimental bench setup for the TEPC	33
Figure 18: TEPC experimental setup.....	34
Figure 19: No shielding versus layers of aluminum on 17 December.....	36
Figure 20: No shielding versus layers of sample X_{woB} on 17 December.....	38
Figure 22: No shielding versus one layer of shielding material on 17 December	40
Figure 23: No shielding versus two layers of shielding material on 17 December.	42
Figure 24: No shielding versus three layers of shielding material on 17 December	43
Figure 25: Histogram plot of the total counts per shielding type..	45
Figure 26: Foil activation spectrum of indium after subtracting the background spectrum.	48
Figure 27: Foil activation spectrum of indium's 336 keV peak corrected for weight, density, and thickness.	49
Figure 28: Foil activation spectrum of zinc after subtracting the background spectrum. This figure shows the results of four separate foil activation experiments.....	51
Figure 29: Foil activation spectrum of zinc's 511 keV peak corrected for weight, density, and thickness, after subtracting the background spectrum	52
Figure 30: Foil activation spectrum of gold after subtracting the background spectrum. This figure shows the results of four separate foil activation experiments.....	54
Figure 31: Foil activation spectrum of gold's 411 keV peak corrected for weight, density, and thickness after subtracting the background spectrum	55
Figure 32: Gas Filling System 1 from Far West	63

Figure 33: No shielding versus layers of aluminum on 18 December.....	66
Figure 34: No shielding versus layers of sample X_{wOB} on 18 December.....	67
Figure 35: No shielding versus layers of sample X_{wB} on 18 December.....	68
Figure 36: No shielding versus one layer of shielding material on 18 December.....	69
Figure 37: No shielding versus two layers of shielding material on 18 December	70
Figure 38: No shielding versus three layers of shielding material on 18 December	71
Figure 39: No shielding versus layers of aluminum on 19 December.....	72
Figure 40: No shielding versus layers of sample X_{wOB} on 19 December.....	73
Figure 41: No shielding versus layers of sample X_{wB} on 19 December	74
Figure 42: No shielding versus one layer of shielding material on 19 December.....	75
Figure 43: No shielding versus two layers of shielding material on 19 December.	76
Figure 44: No shielding versus three layers of shielding material on 19 December	77
Figure 45: No shielding versus layers of aluminum on 20 December.....	78
Figure 46: No shielding versus layers of sample X_{wOB} on 20 December.....	79
Figure 47: No shielding versus layers of sample X_{wB} on 20 December	80
Figure 48: No shielding versus one layer of shielding material on 20 December.....	81
Figure 49: No shielding versus two layers of shielding material on 20 December	82
Figure 50: No shielding versus three layers of shielding material on 20 December	83
Figure 51: Foil activation spectrum of indium for thermal comparison after subtracting the background spectrum	84
Figure 52: Foil activation spectrum of indium's 1097 keV peak corrected for weight, density, and thickness after subtracting the background spectrum.....	85

Figure 53: Foil activation spectrum of indium's 1294 keV corrected for weight, density,
and thickness after subtracting the background spectrum 86

List of Tables

	Page
Table 1: Number of collisions to moderate 2.45 MeV neutrons to 0.025 eV	7
Table 2: Tabulated MCNP Data	16
Table 3: No shielding versus layers of aluminum on 17 December.	37
Table 4: No shielding versus layers of sample X_{w0B} on 17 December.	38
Table 5: No shielding versus layers of sample X_{wB} on 17 December.	39
Table 6: No shielding versus one layer of shielding material on 17 December.	41
Table 7: No shielding versus two layers of shielding material on 17 December.	42
Table 8: No shielding versus three layers of shielding material on 17 December.	44
Table 9: Summary of TEPC data for no shielding and one layer of shielding	47
Table 10: Summary of TEPC data for no shielding and two layers of shielding	47
Table 11: Summary of TEPC data for no shielding and three layers of shielding	47
Table 12: Summary data for indium's 336 keV peak after correcting for weight, density, and thickness	50
Table 13: Summary data for zinc's 511 keV peak after correcting for weight, density, and thickness	53
Table 14: Summary data for gold's 411 keV peak after correcting for weight, density, and thickness	55
Table 15: No shielding versus layers of aluminum on 18 December.	66
Table 16: No shielding versus layers of sample X_{w0B} on 18 December.	67
Table 17: No shielding versus layers of sample X_{wB} on 18 December.	68

Table 18: No shielding versus one layer of shielding material on 18 December.	69
Table 19: No shielding versus two layers of shielding material on 18 December.	70
Table 20: No shielding versus three layers of shielding material on 18 December.	71
Table 21: No shielding versus layers of aluminum on 19 December.	72
Table 22: No shielding versus layers of sample X_{w0B} on 19 December.	73
Table 23: No shielding versus layers of sample X_{wB} on 19 December.	74
Table 24: No shielding versus one layer of shielding material on 19 December.	75
Table 25: No shielding versus two layers of shielding material on 19 December.	76
Table 26: No shielding versus three layers of shielding material on 19 December.	77
Table 27: No shielding versus layers of T6061 on 20 December.	78
Table 28: No shielding versus layers of sample X_{w0B} on 20 December.	79
Table 29: No shielding versus layers of sample X_{wB} on 20 December.	80
Table 30: No shielding versus one layer of shielding material on 20 December.	81
Table 31: No shielding versus two layers of shielding material on 20 December.	82
Table 32: No shielding versus three layers of shielding material on 20 December.	83
Table 33: Summary data for indium's 1097 keV peak after correcting for weight, density, and thickness	85
Table 34: Summary data for indium's 1294 keV peak after correcting for weight, density, and thickness	86

NEUTRON SHIELDING EFFECTIVENESS OF MULTIFUNCTIONAL COMPOSITE MATERIALS

CHAPTER 1 INTRODUCTION

1.1 Background

Rutherford theorized the existence of the neutron in 1920, and in 1932 James Chadwick discovered the neutron by studying a certain type of radiation generated by polonium alpha particles incident on a beryllium target [1]. Originally, Chadwick announced the radiation as “beryllium radiation”, the gamma rays observed would have had to be on the order of 50 MeV to produce the Compton recoil velocities that were recorded. Rutherford could not determine how a 5 MeV alpha particle from polonium deposited on a beryllium target could produce such a large energy gamma ray. By using conservation of momentum and energy, and assuming the mass of the unknown particle was on the order of the proton, Rutherford’s calculations began to make sense. By assuming the particle was without electrical charge as described by Rutherford, Chadwick had discovered the neutron [1].

Neutrons are moderated or reduced in energy by scattering off of nuclei. When cosmic neutrons with high kinetic energy enter earth’s atmosphere, they begin to lose energy through collisions with nitrogen, oxygen, and the mixture of other gas atoms in the atmosphere. Neutrons are especially dangerous to electronic devices because they are a form of non-ionizing radiation that can cause atomic displacements. When neutrons come into contact with electronic components, there is a possibility that electronic

devices will malfunction by lattice dislocation damage in the semiconducting material, resulting in carrier lifetime reduction, carrier concentration reduction, or mobility reduction [2]. Higher neutron fluences correlate to a greater probability that the electronic devices will fail. When the former Soviet Union launched Sputnik into orbit in October 1957 [3], the on-board electronic devices were exposed to a completely different environment than that on earth. As the electronic devices travel further from the earth's atmosphere, power onboard the satellite needs to be conserved. Conserving energy means using low power settings resulting in slow data rate transfer. Because of the slow data rate transfer a single-event upset could occur resulting in the data transfer to be interrupted causing electronic device failure [2].

Satellites are traditionally shielded by encasing the whole vehicle or body in space-grade aluminum. However, the amount of shielding achievable by increasing the aluminum thickness is offset by the added weight and expense to launch the vehicle. Composite materials present an alternative solution to aluminum shielding due to their light weight and ability to incorporate different materials to increase conductivity, radiation shielding, and strengthened mechanical structure.

1.2 Objective of Research

The objective of the research is to investigate and compare the relative neutron shielding capabilities of aluminum and two composite materials. The primary purpose of the research is to validate a simulation of the composite materials and aluminum in a neutron rich environment. The composites materials have constituent atoms designed to absorb and scatter neutrons.

The materials used in the research are laminate nanocomposites made of five different components: carbon fiber, nickel nanostrands, tungsten, boron, and a polymer binder. The two composite samples used in this research contain identical components, but with one major exception; one sample included natural boron (X_{wB}), while the other did not (X_{woB}). The aluminum sample was a piece of T6061 alloy. This thesis compares the shielding effectiveness of the composites and compares them to aluminum.

The primary objective was accomplished by:

1. Developing an MCNP simulation to compare the neutron flux through aluminum and the composite materials.
2. Using a Tissue Equivalent Proportional Counter (TEPC) to measure the relative neutron flux that passes through each material.
3. Conducting fast and thermal neutron foil activation experiments to determine the relative energy dependent neutron shielding effectiveness of the materials.

A secondary objective was to ensure the densities of the composites are equal to or less than that of aluminum. The secondary objective will be accomplished by weighing and measuring the materials to verify their densities, then comparing the calculated results to manufacture-specified values.

It was expected that the composite material with boron would capture more thermal neutrons compared to the other shielding materials. This is because of boron's high cross section for thermal neutron capture. It was expected that the fast neutrons would penetrate the aluminum with few interactions. The composite material without boron should down-scatter the neutrons, but has a small thermal neutron cross section for capturing the slower neutrons compared to the composite material with boron. What is

unclear, and will be shown in this research, is if the composites down-scatter the neutrons enough to allow the fast neutrons to be absorbed in the composite material.

1.3 Paper Organization

In this paper background, theory, experimental design, analysis of experimental data, conclusions, and recommendations for future work will be addressed.

Chapter 1 provides a brief introduction to this study and defines the objectives.

Chapter 2 discusses the theory of neutron moderation through different materials.

Chapter 3 develops the MCNP model for the neutrons penetrating and interacting with different types of shielding materials.

Chapter 4 identifies different experiments conducted to determine the relative shielding capabilities between the different materials.

Chapter 5 analyzes the experimental data.

Chapter 6 is the conclusion of the study and identifies future work.

CHAPTER 2

THEORY

2.1 Overview

This chapter describes how neutrons are moderated in materials. This chapter also identifies how neutrons are attenuated as they travel through different types of materials.

2.2 Moderating Neutrons

Moderating or the slowing down of neutrons is accomplished by repeated collisions of neutrons with the nuclei of the moderating medium. One of the results of a neutron colliding with a nucleus is elastic scattering. Elastic scattering continues to moderate the neutron until the neutrons are captured or pass through the boundaries of the material [1].

Applying conservation of energy and linear momentum, a ratio between E_i and E_{fn} is shown in Equation 2.1 below [4].

$$\frac{E_{fn}}{E_i} = \frac{A^2 + 1 + 2A \cos(\theta)}{(A+1)^2} \quad (0.1)$$

For the simplest case of a neutron colliding head on with a target atom, E_i is the initial energy of the neutron, and E_{fn} is the final energy of the neutron, A is the atomic mass, and θ is the scattering angle. For maximum energy transfer, θ is 180 degrees. Applying $\theta = 180$ degrees, Equation 2.1 becomes:

$$\frac{E_{fn}}{E_i} = \frac{A^2 + 1 - 2A}{(A+1)^2} = \left(\frac{A-1}{A+1} \right)^2 \quad (0.2)$$

Equation 2.2 is utilized for one scatter event of a mono-energetic neutron. After the first collision, the neutron will have a distribution of energies and scattering angles

[4]. In order to make the calculation more quantifiable, ξ is defined as the lethargy. Lethargy represents the average value of $\ln(E_i/E_{fn})$ after a single collision. Equation 2.3 gives the relationship between lethargy and energy, where $d\Omega$ is the element of solid angle in the system between the neutron and the nuclei.

$$\xi = \ln \left[\frac{E_i}{E_{fn}} \right] = \frac{\int \ln \left[\frac{(A+1)^2}{A^2 + 1 + 2 \cos(\theta)} \right] d\Omega}{\int d\Omega} \quad (0.3)$$

After applying the integrals in Equation 2.3, which leaves the particle free to scatter in all directions, we obtain:

$$\xi = 1 + \frac{(A-1)^2}{2A} \ln \left[\frac{A-1}{A+1} \right]. \quad (0.4)$$

The average value of E_{fn} is decreased after each collision, n , by the amount ξ , so after n collisions the average value of $\ln(E_{fn})$ is related to $\ln(E_i)$ by

$$\ln(E_{fn}) = \ln(E_i) - n\xi. \quad (0.5)$$

Rearranging Equation 2.5 to obtain an equation for the number of collisions, given that the material is made of only one isotope, is:

$$n = \frac{1}{\xi} \ln \left(\frac{E_i}{E_{fn}} \right). \quad (0.6)$$

For the elements with natural isotopic ratios in the composite material, and applying Equations 2.4 and 2.6 listed above, Table 1 shows the number of collisions required to moderate a mono-energetic 2.45 MeV neutron to 0.025 eV. In Table 1, A is the atomic mass, ξ is the lethargy, and n is the number collision required.

Table 1: Number of collisions to moderate 2.45 MeV neutrons to 0.025 eV

Element	A	ξ	n
H-1	1.01	1.00	19
C-12	12.00	0.16	117
Ni-58	58.69	0.03	547
W-183	183.84	0.01	1698
Gd-157	157.25	0.01	1453
O-16	16.00	0.12	154
B-11	10.81	0.17	106
Al-27	26.98	0.07	255

2.3 Intensity of Neutrons through a Material

Neutrons are moderated through a material by interacting with other nuclei, as discussed in Section 2.2. This section will study the simplest case of the intensity of the detected neutrons that pass through a composite material. Assuming a narrow beam of mono-energetic 2.45 MeV neutrons (from a deuterium-deuterium (D+D) reaction) passes through the material, and the intensity of the neutrons can be measured when it leaves the composite material, Knoll states the relation shown in Equation 2.7 [5].

$$\frac{I}{I_0} = e^{-\Sigma_{tot}t} \quad (0.7)$$

Equation 2.7 calculates the fraction of the neutron beam that passes through the material without interacting. In Equation 2.7, I is the final intensity of the neutron, I_0 is the initial intensity of the neutron, Σ_{tot} is the total macroscopic cross section, which represents the probability of an interaction per centimeter, and t represents the thickness of the material. When there is more than one type of material that the neutron will come into contact with, Equation 2.8 needs to be applied to Equation 2.7.

$$\Sigma_{tot}t = \sum_{i=1}^{\#Isotopes} \sigma_i N_i t_i \quad (0.8)$$

In Equation 2.8 $\sum_{tot} t$ is equal to the summation of the composite materials individual isotope layers, $\# Isotopes$ represents the number of isotopes in the composite material; σ_i is the microscopic cross section, which represents the probability of an interaction in barns or cm^2 ; N_i represents the total number of atoms per unit volume of that particular isotope; and t_i represents the thickness of the individual isotope in the composite material.

Applying Equation 2.8 to Equation 2.7 with a total thickness of 2.54 cm the composite materials and aluminum, I/I_0 becomes 94.29% for sample X_{wB} , 95.69% for sample X_{woB} , and 77.9 % for T6061, representing the percentages of the mono-energetic 2.45 MeV neutrons that pass through each material without interacting. What this calculation shows is that aluminum allows the fewest number of 2.45 MeV neutrons through the different types of shielding materials without interacting. Normally, neutrons are not collimated in a narrow beam, which means Equations 2.6, 2.7, and 2.8 are not accurate except for the theoretical case stated above. A modeling program is therefore used to get a more accurate estimate of the neutron flux through the shielding materials.

CHAPTER 3

MODELING

3.1 Introduction

MCNP (Monte Carlo Neutral-Particle) is a general purpose simulation code that can be used for neutron, photon, electron, or coupled neutron/photon/electron transport. Specific areas of application include, but are not limited to, radiation protection and dosimetry, radiation shielding, radiography, medical physics, nuclear criticality safety, detector design and analysis, accelerator target design, fission and fusion reactor design, and decontamination and decommissioning [6].

MCNP was used to simulate a mono-energetic, mono-directional 2.45 MeV neutron source that penetrated the composites and the aluminum. By comparing the results for the three different types of simulations, a prediction can be made to determine how the materials will shield against fast neutrons.

3.2 Assumptions

With the information and specifications originally provided by the manufacturer on the content of the composites, a MATLAB code was developed to calculate the density of the material and the weight percentage of each element in the material. Density and weight of the shielding material are critical in developing the most accurate code to model this shielding material. Figure 1 illustrates the model used in the MCNP simulations.

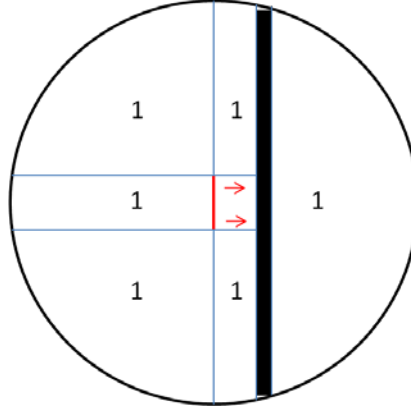


Figure 1: Illustration of the model used in MCNP. The red line represents a 1 cm² planar source. The source is mono-directional to the right. The large black rectangle represents the shielding material. Its dimensions are 199.96 x 199.96 x 2.54 cm. The ones represents all space in which MCNP tracks the path of the neutrons.

The source was a 1 cm² mono-directional planar source centered at the origin, located 0.1 cm from the shielding material. The source neutron energy was 2.45 MeV, simulating the D-D neutron flux. The simulation volume was modeled as a sphere centered at the origin with a radius of 100 cm. The shielding material was modeled as a large, thin rectangle with dimensions of 199.96 cm² by 2.54 cm thick. The large size is needed to minimize the amount of neutrons that escape through the sides, rather than exit through the backside of the material. The simulation volume is in a vacuum, and the neutrons are tracked as long as they remain inside the sphere, but are killed or no longer tracked when they leave the sphere [7].

All three shielding materials were modeled in the same way for comparison; one denoted as sample X_{wB}, one as sample X_{woB}, and the last aluminum. Utilizing data from the manufacturer, the calculated weight percentages in sample X_{wB} is: 26.00% carbon, 19.79% nickel, 21.19% tungsten, 25.46% natural boron, 1.48% hydrogen, 4.64% oxygen, 0.72% nitrogen, and 0.72% sulfur. The calculated weight percentages in sample X_{woB} is:

25.67% carbon, 31.21% nickel, 33.43% tungsten, 2.26% hydrogen, 5.89% oxygen, 0.77% nitrogen, and 0.77% sulfur. The calculated weight percentages of T6061 is: 97.29% aluminum, 0.15% titanium, 0.25% zinc, 0.35% chromium, 0.12% magnesium, 0.15% manganese, 0.40% copper, 0.80% silicon, and 0.07% iron [8]. These values were used to model the material in each simulation.

One of the parameters that is variable in MCNP is the number of particles the model uses in its statistical analysis. Sample X is a generic model for the composite material that was developed prior to the codes for sample X_{wOB} and sample X_{wB} . Sample X is not the most accurate representation of the composite material, but is shown to illustrate the amount of time required to run a model based on the number of incident particles versus the relative error in the distribution of points (Figure 2).

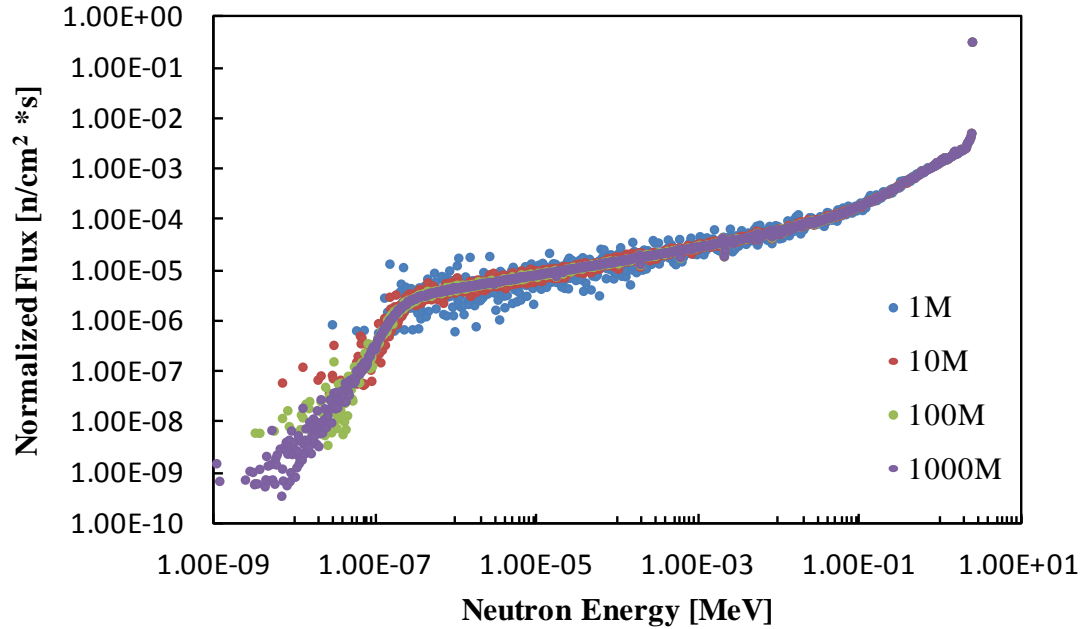


Figure 2: MCNP results that illustrate the accuracy of the simulation versus the amount of time to run a simulation. The blue dots represent a simulation with one million particles that took 0.23 minutes. The red dots represent a simulation with ten million particles that took 1.59 minutes. The yellow dots represent a simulation with one hundred million particles that took 14.9 minutes. The purple dots represent a simulation with one billion particles that took 149.5 minutes.

In Figure 2, a larger number of incident particles simulated results in a smaller data distribution, but required more time. Additionally, all simulations have a smaller distribution of data points at high neutron energies. This is due to the lower relative error associated with the data points at higher neutron energies, where there are more counts. To eliminate the large uncertainties, more particles are needed in the simulations to decrease the relative error. For this research, the simulations were conducted with 10 million particles, because the time to run each simulation was approximately 1.59 minutes, and many simulations could be run in a reasonable amount of time.

The material density was determined using a scale accurate to ± 0.001 of a gram. A digital micrometer was used to measure the volume of the sample. A density of 2.40

grams/cm³ was calculated for sample X_{wB}, a density of 1.77 grams/cm³ was calculated for sample X_{wOB}, and a density of 2.66 grams/cm³ was calculated for aluminum.

3.3 Modeling Results and Analysis

For all simulations, 10 million particles were used, and a surface flux tally (F2) was measured on the back side of the target material. The surface flux is the amount of particles that cross the back side of the material per unit area per second. All of the results are normalized, and key data from each figure are found in the figure caption and in Table 2. The dimensions of the target material were the same as those illustrated in Figure 1 from Section 3.2.

The simulation of the aluminum is shown below in Figure 3.

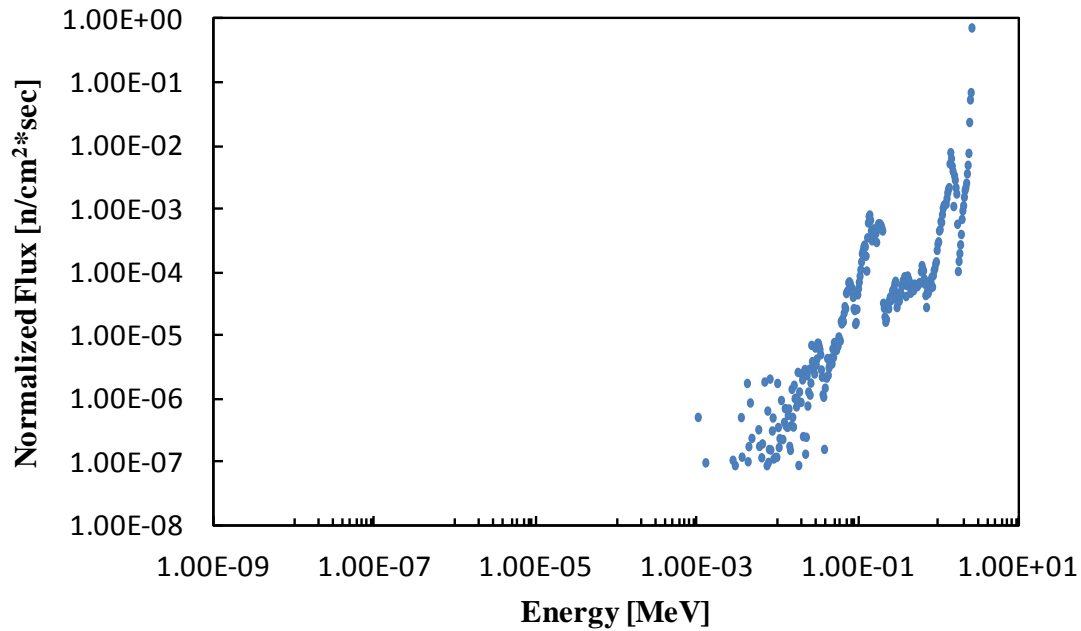


Figure 3: MCNP simulation for T6061 aluminum. Ten million particles were used in this simulation; 99.989% of the neutrons made it through the material and 0.011% were captured. Of the total number of neutrons that made it through the material, 85.9% remained at the incident energy of 2.45 MeV.

As shown in Figure 3, aluminum does not stop or slow down 2.45 MeV neutrons due to its very low scattering cross section and neutron energy transfer per collision for fast neutrons. Figure 4 is the simulation results with sample X_{woB} as the target material.

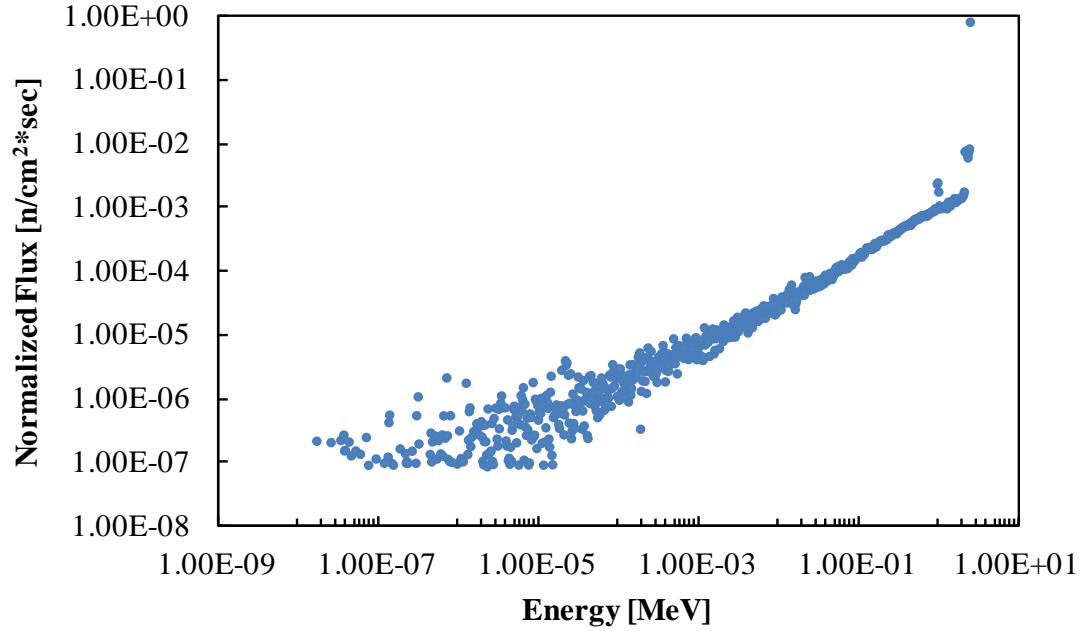


Figure 4: MCNP simulation for sample X_{woB} . Ten million particles were used in this simulation; 99.911% of the neutrons made it through the material and 0.089% were captured. Of the total number of neutrons that made it through the material, 83.6% remained at the incident energy of 2.45 MeV.

The simulation results with sample X_{wB} are shown in Figure 5. The simulated results showed that sample X_{wB} outperformed sample X_{woB} in the number of captures as natural boron was added to the composite material.

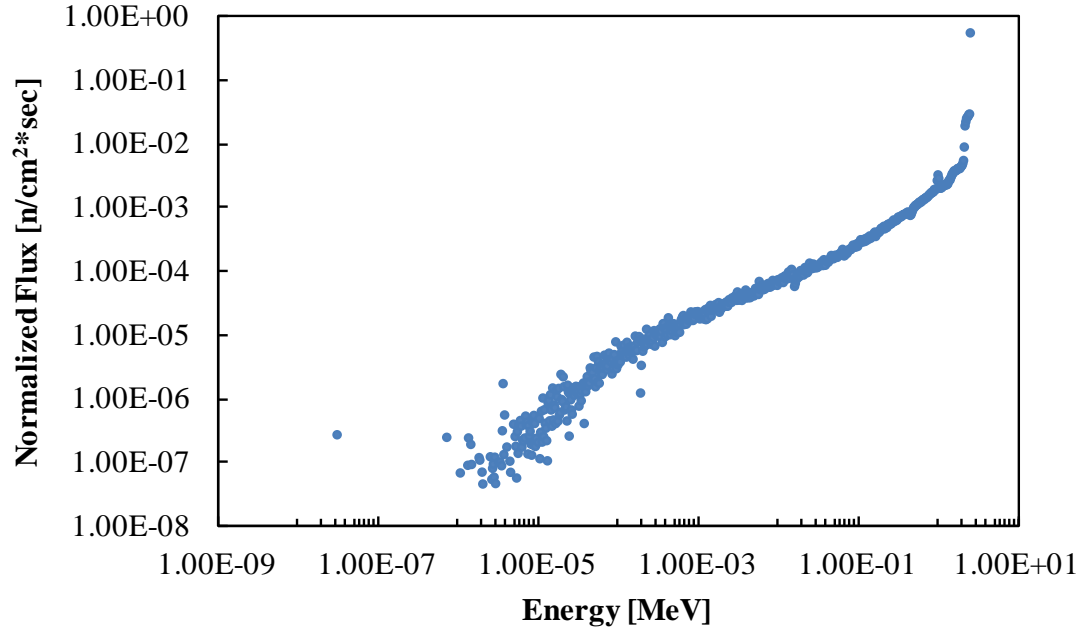


Figure 5: MCNP simulation for sample X_{wB} . Ten million particles were used in this simulation; 98.276% of the neutrons made it through the material and 1.724% were captured. Of the total amount of neutrons that made it through the material, 57.50% remained at the incident energy of 2.45 MeV.

Figure 6 shows all three simulations in one plot. This figure shows that T6061 compared to the composites has the least down-scattering for the 2.45 MeV neutrons, and shows that there is a cutoff at thermal energies for sample X_{wB} due to thermal neutron absorption in the boron.

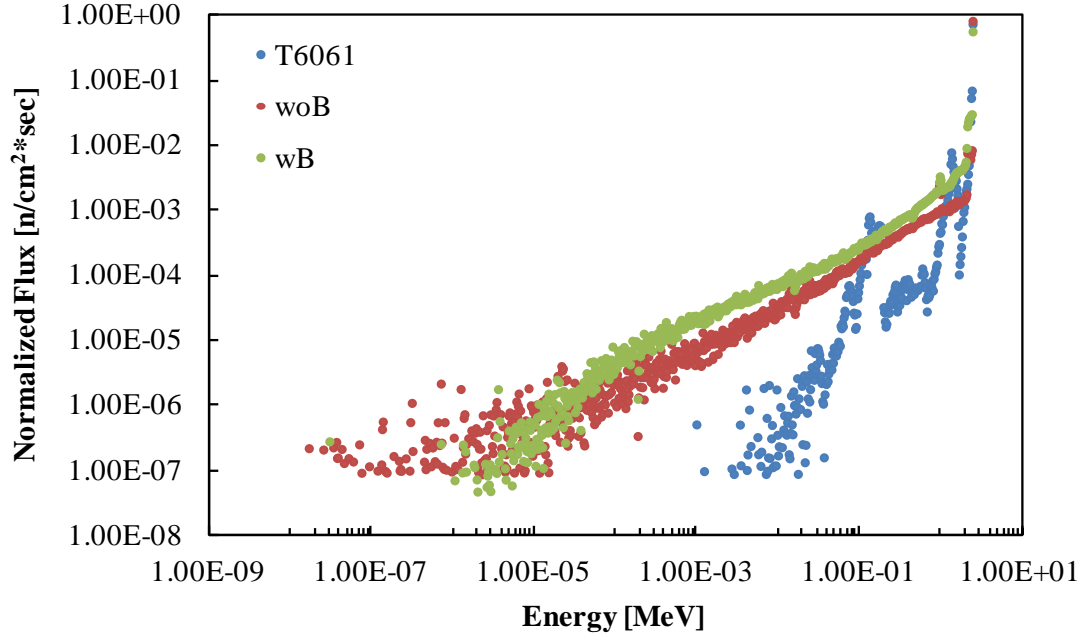


Figure 6: Combination plot of all MCNP simulations. The blue dots represent T6061 simulation. The red dots represent sample X_{woB} . The green dots represent sample X_{wB} .

Table 2 below shows the tabulated results of the simulations.

Table 2: Tabulated MCNP Data

Material	Density [g/cm ³]	Percent Captured	Percent Transmitted without Interacting	Percent Transmitted Normalized to T6061
Al (T6061)	2.66	0.01	85.90	99.98
Sample X_{woB}	1.77	0.09	83.60	66.44
Sample X_{wB}	2.40	1.72	57.50	88.67

From Table 2, the sample material with boron captures the greatest percentage of neutrons, and produces the most down-scattering. In the last column in Table 2, the percent transmitted is calculated with the densities of sample X_{woB} and sample X_{wB} normalized to the density of T6061 aluminum. By doing this normalization, a comparison between the amounts of neutrons transmitted compared to T6061 can more

accurately be represented. At normalized densities, sample X_{woB} allows the fewest amount of neutrons through the material.

Gadolinium has a higher thermal neutrons absorption cross section than boron. However, it takes natural gadolinium 1453 collisions to moderate 2.45 MeV neutrons to thermal energies, but it takes natural boron only 106 collisions to moderate the same neutron to thermal energies (Table 1). Gadolinium's cross section for capturing thermal neutrons is extremely high, approximately two orders of magnitude higher than boron, but is on the same order of magnitude when considering fast neutrons. Boron-11 and carbon-12 have similar cross sections for absorption over all incident energies. The cross section of aluminium-27 is roughly one order of magnitude less than boron-11 and carbon-12 until the incident energies reach approximately 1 MeV. Figure 7 shows the total neutron cross sections for the natural isotopes of boron-10, boron-11, carbon-12, aluminum-27, and gadolinium-157 [9].

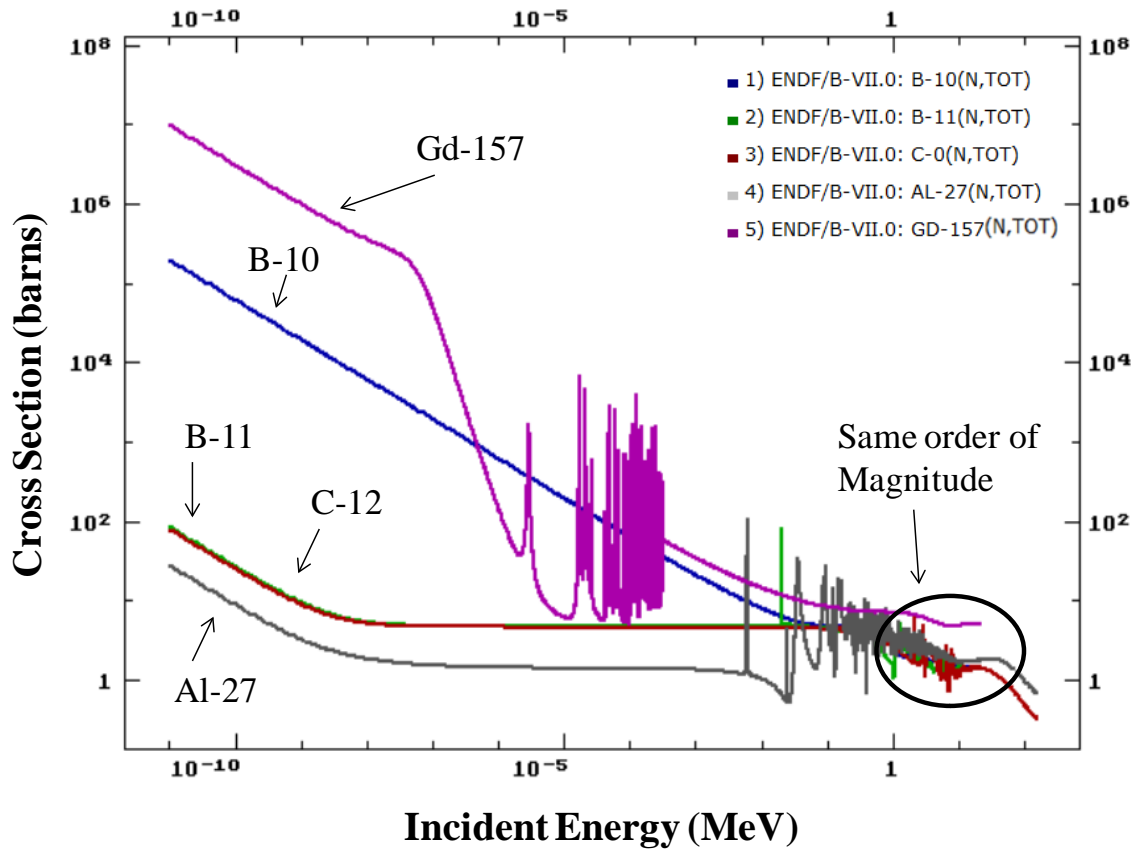


Figure 7: Total neutron cross section for boron and gadolinium from ENDF. Boron 10 and boron 11 are labeled in this figure, all other lines are gadolinium. At the higher energies, the boron and gadolinium cross sections are very similar. At the lower energies 10^{-8} MeV (thermal energy), boron is at times several orders of magnitude lower in cross section than gadolinium.

As described in Section 2.2 and shown in Figure 7, boron seems more effective when used in the composite material. Natural boron does not have as high thermal neutron capture cross section as gadolinium-157. However, its capture cross section is higher than most elements. By moderating the fast neutrons they have a higher probability of being captured. Boron's ability to moderate fast neutrons is a tremendous advantage over gadolinium. If gadolinium was to be used instead of natural boron with the same thickness of material, 2.54 cm, the density of the composite material would change from 2.4 g/cm^3 to 9.68 g/cm^3 . This change in density could potentially add a

tremendous amount of weight to a satellite system resulting in increased launch costs. For this reason, boron is the better choice for the composite materials.

There is an engineering compromise to the amount of boron that could be added to the material to optimize the amount of neutron captures in the material, the percent of neutrons that make it through the material, and the amount of neutrons that make it through the material at 2.45 MeV. Examining Table 2, sample X_{wB} has the greatest number of captures at one-inch thickness. Figure 8 shows the fraction of neutrons captured as a function of composite material thickness for sample X_{wB} (blue dots).

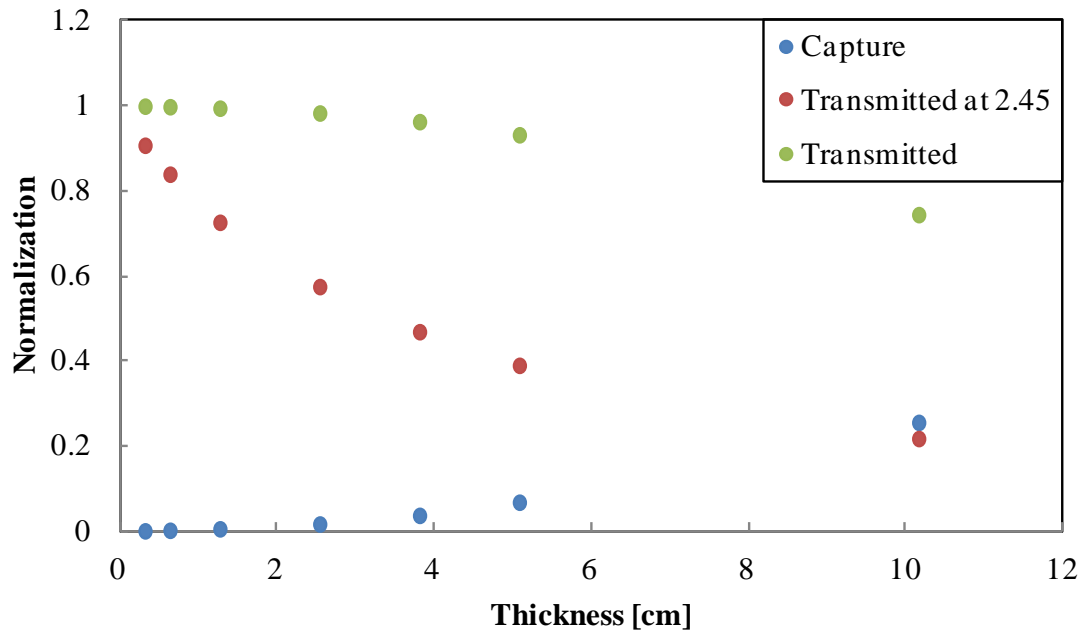


Figure 8: Engineering limit combination plot. The blue dots represent the fraction of neutrons captured in sample X_{wB} as a function of composite material thickness. The green dots represent the fraction of total neutrons through sample X_{wB} . With increasing composite material thickness, the fraction of total neutrons that makes it through the material continues to decrease. The red dots represent the fraction of 2.45 MeV neutrons that makes it through sample X_{wB} . For increasing sample thickness, the amount of 2.45 MeV neutrons that makes it through the material continues to decrease. The fraction of 2.45 MeV neutrons that makes it through the material will continue to decrease with increasing thickness until it reaches 0%.

Figure 8 shows the fraction of total neutrons that are transmitted through the sample X_{wB} as a function of thickness (green dots). With increasing composite material thickness, the fraction of total neutrons that makes it through the material continues to decrease. Figure 8 also shows the fraction of 2.45 MeV neutrons that makes it through sample X_{wB} (red dots). For increasing sample thickness, the amount of 2.45 MeV neutrons that make it through the material continues to decrease.

As a result of Figure 8, increasing the thickness of the composite material results in a better performance in the overall neutron shielding. Thicker samples could be tested, but there is a trade-off in the use of thicker samples due to their increased weight.

3.4 Modeling Conclusion

After evaluating the MCNP simulations, when not normalizing the composites density and thickness to T6061, sample X_{wB} is the best for shielding neutrons, when normalizing the density and thickness sample X_{woB} seems to outperform T6061 and sample X_{wB} . There are differences between all three shielding materials that should be distinguishable in the experimental results. In the next chapter, two types of experiments are proposed to measure the relative differences in neutron shielding effectiveness of aluminum and the two composite materials, sample X_{woB} and sample X_{wB} . These two composites and aluminum should result in statistically significant differences in neutron shielding effectiveness.

CHAPTER 4

EXPERIMENT

4.1 Introduction

Two experiments are discussed in this chapter; one that involves using foil activation and one that involves using a tissue equivalent proportional counter. Both experiments identify the number of counts detected, and will allow for a relative changes between aluminum and the composite materials tested. Both experiments were originally planned to be conducted at AFIT's D+D neutron generator, but during the preliminary experimental setup and development of these procedures, the D+D neutron generator malfunctioned, preventing the completion of the experiments. As a result, a plutonium-beryllium (PuBe) neutron source was substituted for the remaining experimental runs.

4.2 Foil Activation Experiment

Before the experiment was moved to the PuBe source, a calculation was conducted to calculate the overall activity of the shielding material. When the materials are exposed to neutrons, there is a possibility of activating them. The D+D neutron generator produces an approximate total neutron flux of 1×10^8 neutrons/cm²-s, and the neutrons are emitted isotropically from a volumetric cone. Using a previously developed mathematical code [10], a calculated activity of the shielding materials was determined as shown in Figures 9 through 11 for a consistent sample size of 2.29 x 1.02 x 0.39 cm. Figures 9 through 11 presents the results of the activity calculations from sample X_{wB}, sample X_{woB}, and aluminum as a function of time, from the start of irradiation to 16 hours

after irradiation, with an irradiation time of 36000 seconds (10 hours), with a flux of approximately 1×10^8 neutrons/cm²-s.

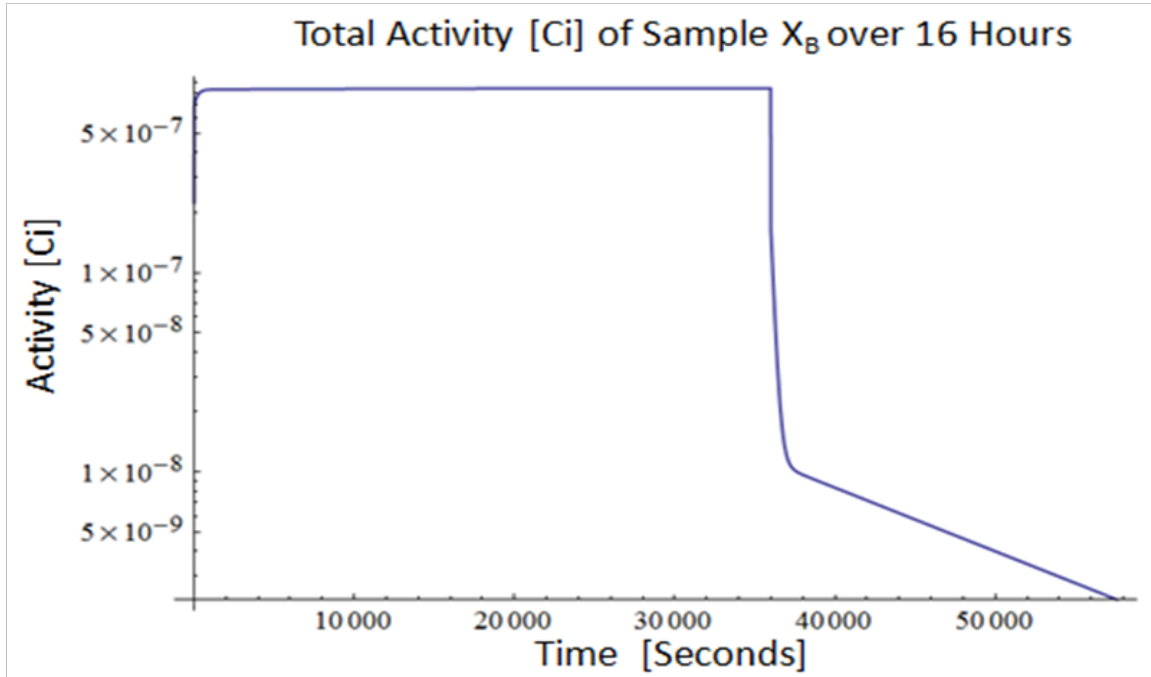


Figure 9: Total activity of sample X_{wB}, 16 hours following a 10 hour irradiation with a neutron flux of 1×10^8 neutrons/cm²/sec.

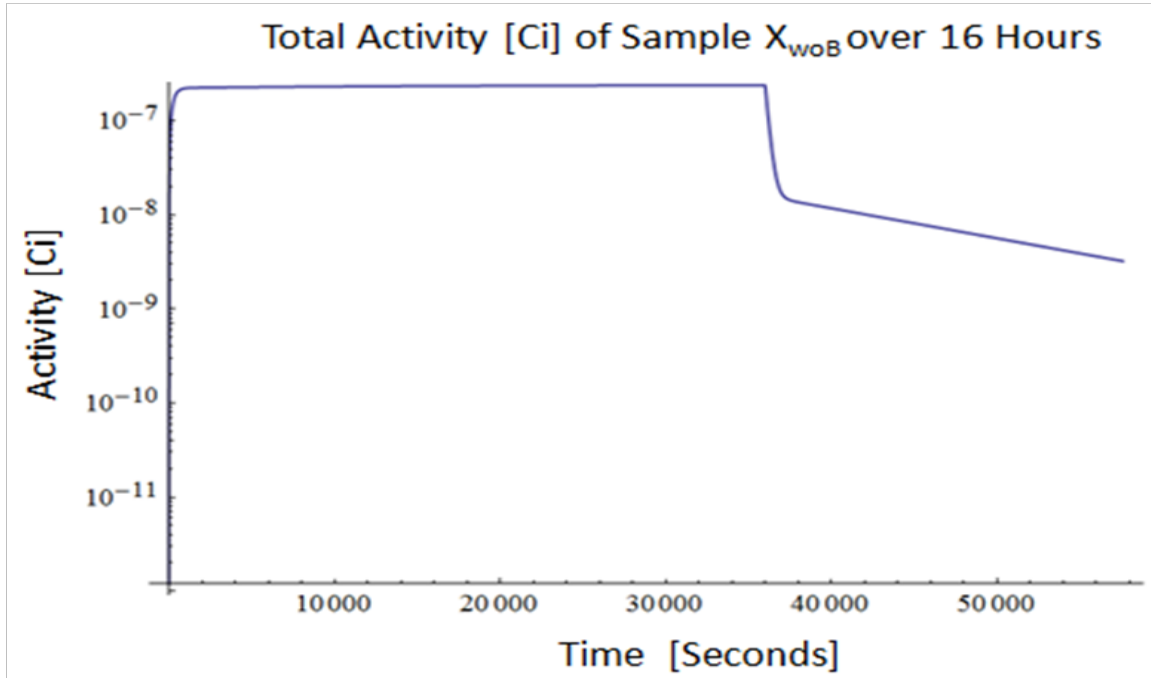


Figure 10: Total activity of sample X_{woB} , 16 hours following a 10 hour irradiation with a neutron flux of 1×10^8 neutrons/cm²/sec.

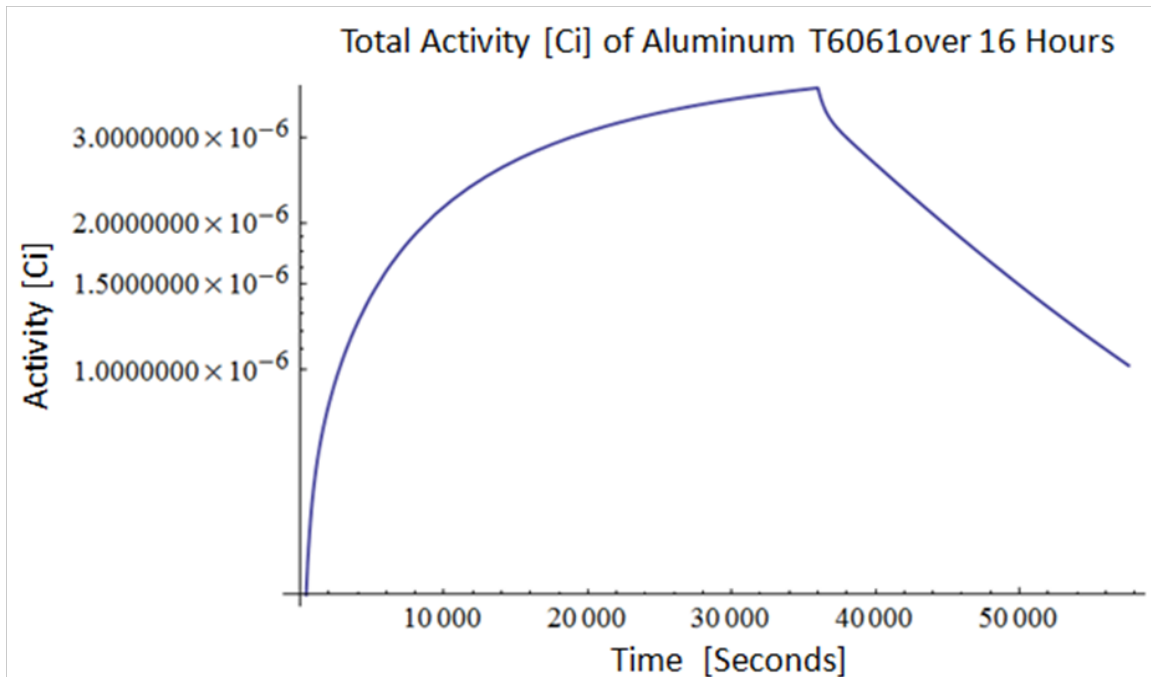


Figure 11: Total activity of T6061, 16 hours following a 10 hour irradiation with a neutron flux of 1×10^8 neutrons/cm²/sec.

The maximum activity from Figures 9 and 10 during irradiation for sample X_{wB} was calculated to be 8.4×10^{-7} Ci, and for sample X_{woB} was calculated to be 2.4×10^{-7} Ci. The maximum activity for aluminum from Figure 11 was calculated to be 3.8×10^{-6} Ci. All three samples were not significantly radioactive, but during the extraction of the materials, handling time was limited to reduce the overall exposure. Figures 9 through 11 were calculated using the D+D neutron generator as the source. Because these activities were so low, when the decision was made to move to the PuBe source, the activity of the shielding materials was not recalculated.

The foil activation experiment was conducted using a PuBe source (cylindrical 4.678 Ci source, with dimensions 0.82 inch diameter and 3.72 inch height), with activation data acquired using a well-type High Purity Germanium (HPGe) detector. The PuBe source produces a spectrum of neutrons from 0.5 to 10 MeV, with a typical flux of approximately 1×10^7 neutrons/cm²-s [1]. Figure 12 shows a typical Pu-Be spectrum of neutrons.

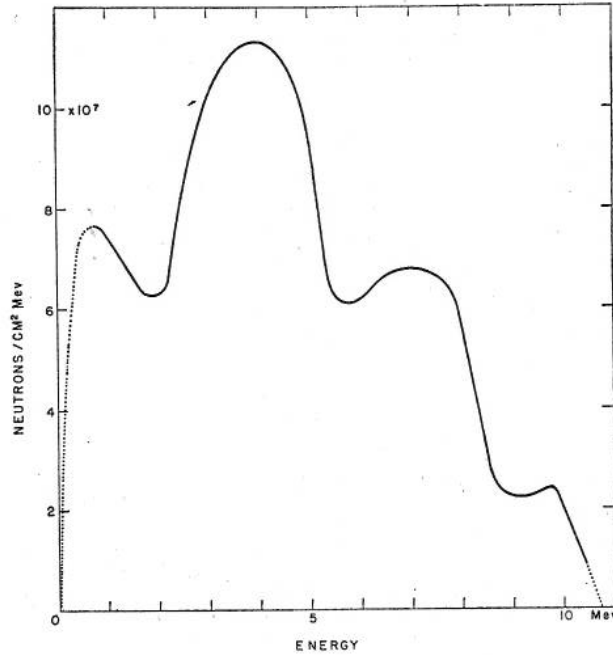
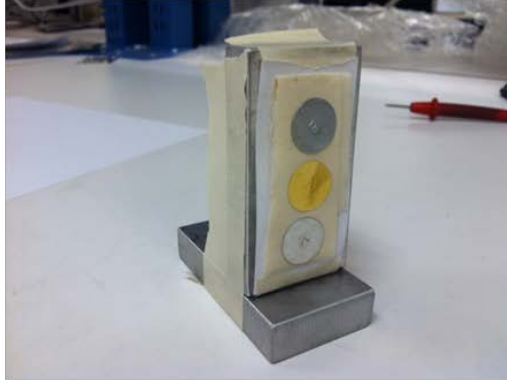
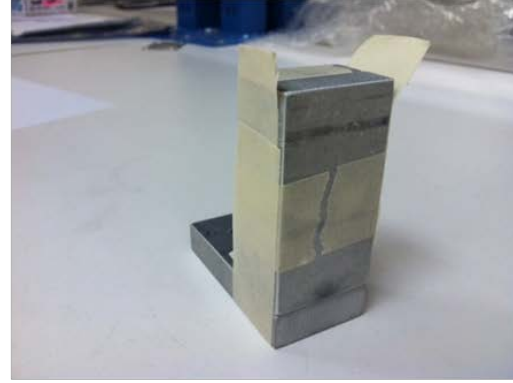


Figure 12: PuBe neutron source spectrum. The spectrum is from approximately 0.5 MeV to 10 MeV [1]. Black lines are experimental confirmed, and the dashed lines are extrapolated zero fluence.

The PuBe source is a cylindrical source and it is assumed to be isotropic [11]. One set of foil samples were placed vertically in front of the PuBe source, and the experiment was conducted four times. The first time, the foils were not sandwiched between the shielding materials to allow for a non-shielded response. In the next experiment aluminum was used as the shielding material. The third and fourth experiments were conducted with the composite materials sample X_{wOB} and sample X_{wB} , respectively. Figure 13 depicts the experimental setup for the foil activation, and shows how the foils were adhered between the shielding materials and placed in front of the PuBe source. In Figure 13, aluminum is the shielding material, but similar setups were constructed with sample X_{wOB} and sample X_{wB} .



(A)



(B)



(C)

Figure 13: Experimental setup for foil activation using the PuBe source in building 470. Figure (A) shows how the foils were adhered to the shielding material. Figure (B) show the foils totally enclosed in the shielding material. Figure (C) shows the foils being irradiated by the Pu-Be source.

Each foil activation experiment consisted of 13.25 hours of irradiation using the PuBe source, followed by 10.5 hours of counting time in the HPGe detector. The results of this experiment are discussed in Chapter 5, Section 2. The foils used for each experiment were gold (Au), zinc (Zn), and indium (In). Each of the three foils, when activated by neutrons, decays with specific gamma ray peaks. The gold foil, with an isotopic composition of 100% ^{197}Au [5], was used to detect thermal neutrons. When ^{197}Au absorbs a thermal neutron, it becomes ^{198}Au with a half-life of 2.695 days and

decays by β^- to ^{198}Hg , which subsequently de-excites by emitting a 411.8 keV gamma ray.

Using foils to detect fast neutrons is difficult because most foils have a very low probability, or cross section, for absorbing fast or high energy neutrons. Threshold activation is a special type of reaction that occurs when fast neutrons interact with foils, and the use of the threshold reaction is the best method for detecting fast neutrons when conducting foil activation experiments. In the natural zinc foil, ^{64}Zn has an isotopic abundance of 37.8%. The reaction of interest is $^{64}\text{Zn}(n,p)^{64}\text{Cu}$, where ^{64}Cu has a half-life of 12.7 hours [5]. When this reaction occurs a positron annihilation releases a 511 keV gamma ray. The threshold energy for this reaction is approximately 2.0 MeV. The indium foil, ^{115}In has an isotopic abundance of 95.7% of natural indium. The reaction of interest is $^{115}\text{In}(n,n')^{115m}\text{In}$, where ^{115m}In has a half-life of 4.5 hours [5]. When the neutron impacts the indium nuclei, it transfers some of its energy to the indium atom, putting some energy in an excited state. When the nuclei de-excites to the ground state it releases a 336 keV gamma ray is released. The threshold energy for this reaction is approximately 0.5 MeV.

The foils were exposed for 13.25 hours to the PuBe source then extracted and immediately transported to the HPGe detectors. The indium and zinc foils were placed in the HPGe detectors and counting started first. The total elapsed time between removing the foils and starting the counting was four minutes, every time the experiment was conducted. After the indium and zinc foils counting time had started, the gold foil was transported to HPGe detector located in a separate building. The total elapsed time between removing the gold foil and starting the count in the HPGe detector was 10

minutes, or 6 minutes after counting of the indium and zinc foils commenced. After a 10.5 hour count time was complete, a comparison between the counts for all three foils was conducted to determine a relative count difference between aluminum, sample X_{woB} , and sample X_{wB} , at the three different gamma ray peaks. The results shown in Chapter 5, Section 2 compare the relative shielding effectiveness of aluminum, sample X_{woB} , and sample X_{wB} for fast and thermal neutrons. Also, Appendix D contains the results of evaluating two of indium's thermal peaks.

4.3 Tissue Equivalent Proportional Counter Experiment

A tissue equivalent proportional counter (TEPC) is a proportional counter that detects fast neutrons. The TEPC detector's walls and fill gas mixture mimics the elemental composition of biological tissue [5]. The walls of the TEPC are conducting tissue equivalent plastic, and the gas is methane. When a fast neutron enters the detector and moves through the gas, the neutron loses very little to no energy because the density of the gas is extremely low. After the neutron passes through the gas, it contacts the wall of a plastic sphere at the center of the detector, and the neutron potentially interacts with the hydrogen in the plastic resulting in a recoil proton. That recoil proton ionizes the methane, the free electrons from the methane molecules are collected at the anode due to the applied electric potential. The anode signal is collected in the preamplifier the signal is sent to a multichannel analyzer (MCA), and from the MCA, a signal is sent to Gamma Vision [12]. The resulting graph is a recoil proton spectrum. Figure 14 illustrates the recoil proton spectrum for ^{252}Cf provided by the TEPC manufacturer, Far West [13].

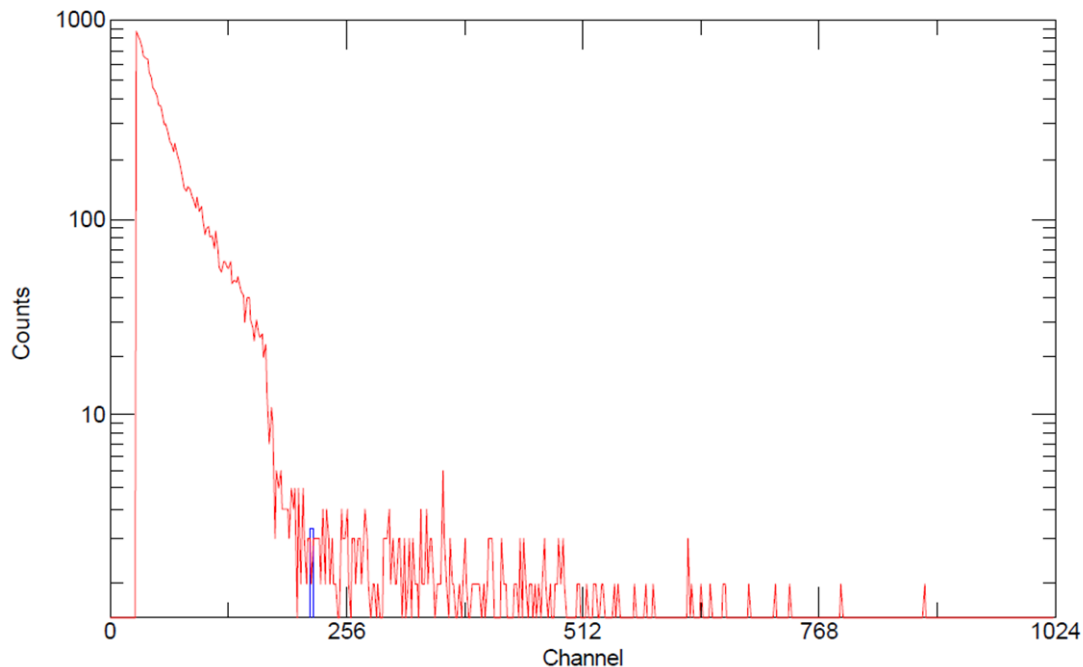


Figure 14: Recoil proton spectrum for ^{252}Cf .

The TEPC is just a detector, but there is another critical piece of equipment, called the gas filling system (GFS-1), that needs to be mastered before any experiment can be used with the TEPC. The GFS-1 seen in Figure 15 is an important component of the experimental setup. By using the manufacturer's instructions for filling the TEPC, and prior experience from the Air Force Radiological Assessment Team (AFRAT), a detailed step-by-step filling checklist can be found in Appendix B for follow-on students to use.

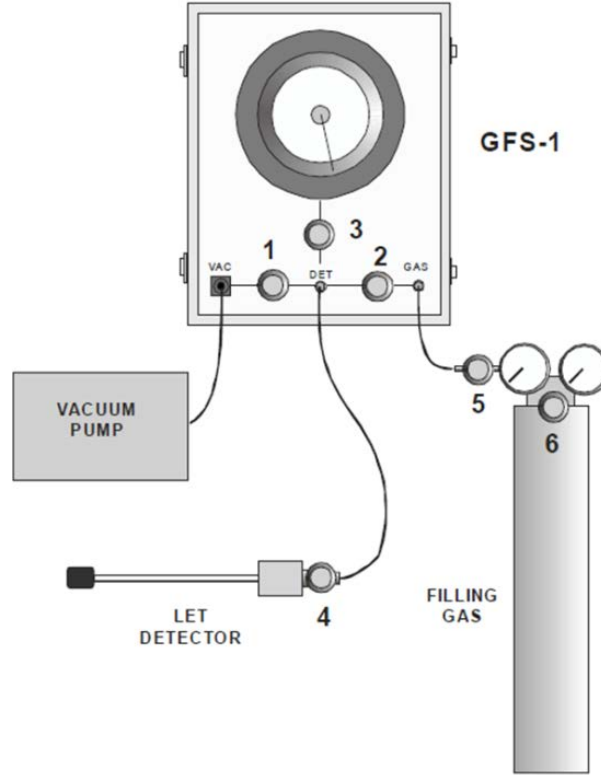


Figure 15: Setup of the TEPC with the gas filling system. Number 1 is the valve for the vacuum pump. Number 2 is the valve that goes to the fill gas. Number 3 is the valve for the pressure meter. Number 4 is the valve for the detector. Number 5 lets the gas flow out of the fill gas canister. Number 6 is the valve that opens or closes the fill gas [14].

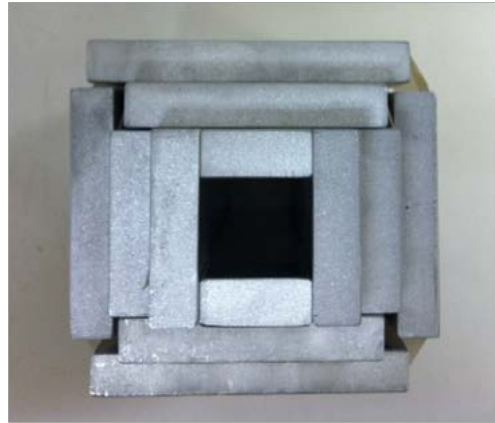
A PuBe source that was used for the TEPC experiment is the same PuBe source used in the foil activation experiments. Because the TEPC experiment only used half of the possible neutron that the PuBe source produces, the neutron fluence is approximately 5×10^6 neutrons/cm². When looking at the solid angle of the shielding material to the PuBe source, the front side of the shield is as large as the PuBe source, so for these experiments, half the total fluence will be used. Though this is not as high of a neutron fluence, as the D+D neutron generator, the PuBe source produces a spectrum of neutrons from 0.5 to 10 MeV. For the experiment, the TEPC was placed 3.33 cm in front of the

PuBe source to allow for the shielding material to be placed between the source and the detector. The LET spectrum was recorded using Gamma Vision software [12].

Figure 16 shows a close-up view of the shielding box used in the TEPC experiments. Figure 17 shows an experimental bench setup with the TEPC. In Figures 16 and 17, the shield is aluminum and in Figure 18 the shield is sample X_{woB} . Figure 18 illustrates the box configurations with no shielding, one layer of shielding, two layers of shielding, and three layers of shielding. Similar boxes were used for sample X_{woB} , sample X_{wB} , and aluminum. The experiment consisted of placing the TEPC in front of the Pu-Be source for 3600 seconds as shown in Figure 18 (B). Three layers of a five sided box were placed around the TEPC as shown in Figure 18 (D). The TEPC was then returned back in front of the Pu-Be source for 3600 seconds and the results were recorded. When the time concluded, the outermost shielding material layer was removed. Next, two layers of the box were placed over the TEPC, and the TEPC was placed back in front of the PuBe source for another 3600 seconds, as shown in Figure 18 (E). Upon completion of the experiment, the outermost layers of shielding material were removed. Finally, a single-layered box was placed over the TEPC and placed in front of the PuBe source for another 3600 seconds, as shown in Figure 18 (F). This process was repeated for aluminum and sample X_{wB} . The results of the TEPC experiments are discussed in Chapter 5, Section 1.



(A)

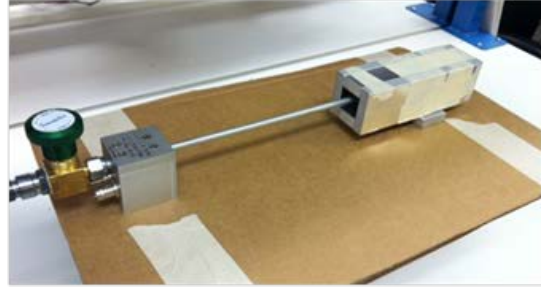


(B)

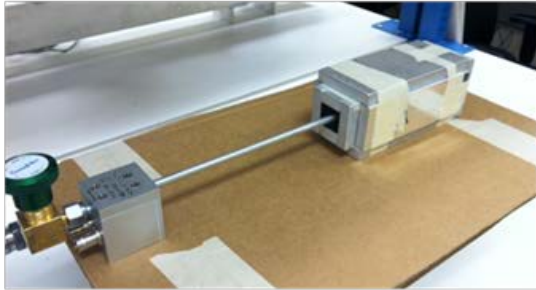
Figure 16: Close-up view of the three layer shielding box. Figure (A) is a side profile of the shielding box. Figure (B) is the rear view TEPC shielding box. In the center of the box is where the TEPC is inserted.



(A)



(B)



(C)



(D)

Figure 17: Experimental bench setup for the TEPC. Figure (A) is the setup with no shielding. Figure (B) is the experimental setup with one layer of shielding with the TEPC inserted. Figure (C) is the experimental setup with two layers of shielding with the TEPC inserted. Figure (D) is the experimental setup with three layers of shielding with the TEPC inserted.



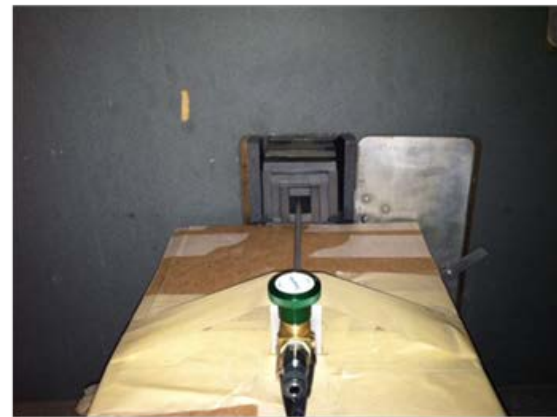
(A)



(B)



(C)



(D)



(E)



(F)

Figure 18: TEPC experimental setup. Figure (A) is the where the TEPC was placed on the stand each time. Figure (B) is the TEPC taped to the stand. Figure (C) is the setup with no shielding in front of the Pu-Be source. Figure (D), (E), and (F) is the experimental setup with three, two, and one layers respectively of sample X_{wB} shielding with the TEPC inserted.

CHAPTER 5

EXPERIMENTAL RESULTS AND ANALYSIS

5.1 Tissue Equivalent Proportional Counter Experiment

The TEPC experiments were conducted 17 through 20 December 2012 in the basement of building 470 using the PuBe source. The plots shown in this section are only for 17 December because each day was a repeat of the experiment for statistical purposes. Plots and tabulated data for 18 through 20 December are shown in Appendix C.

5.1.1 Aluminum Shielding with TEPC

The TEPC with no shielding established a base-line of how many detectable recoil protons are produced by the unshielded source. In all plots found in Section 5.1, the TEPC with no shielding was used as a base-line to compare the different types of shielding materials. Figure 19 shows the TEPC with no shield against one, two, and three layers of aluminum. The most noticeable result was that three layers of aluminum shielded worse than two layers of aluminum shielding. In subsequent tests, two layers of aluminum shielding performed worse than one layer of the aluminum shielding. In all tests, the additional layers of aluminum shielding provided a larger area for neutron interaction, which allowed the TEPC to have a greater probability for a neutron collision inside the detector. Table 3 shows the tabulated data that coincides with Figure 19. The summation of the counts under each curve was taken per experiment and applied to Equation 5.1 to give a percentage difference in shielding, where P is the percent difference between NS (no shielding) and LS (layered shielding) for that experiment.

$$P = \left(\frac{\text{abs}(NS - LS)}{NS} \right) * 100 \quad (5.1)$$

Equation 5.2 gives the general form of the error propagation, and Equation 5.3 gives the error propagation for Equation 5.1, where σ is the standard deviation, σ^2 is the variance, and the subscripts correspond to no shielding and layered shielding [5].

$$\sigma_P^2 = \sum_i \left(\frac{\partial P}{\partial x_i} \right)^2 \sigma_{x_i}^2 \quad (5.2)$$

$$\sigma_P = \sqrt{\left(\frac{-LS}{NS^2} \right)^2 \sigma_{NS}^2 + \left(-\frac{1}{NS} \right)^2 \sigma_{LS}^2} \quad (5.3)$$

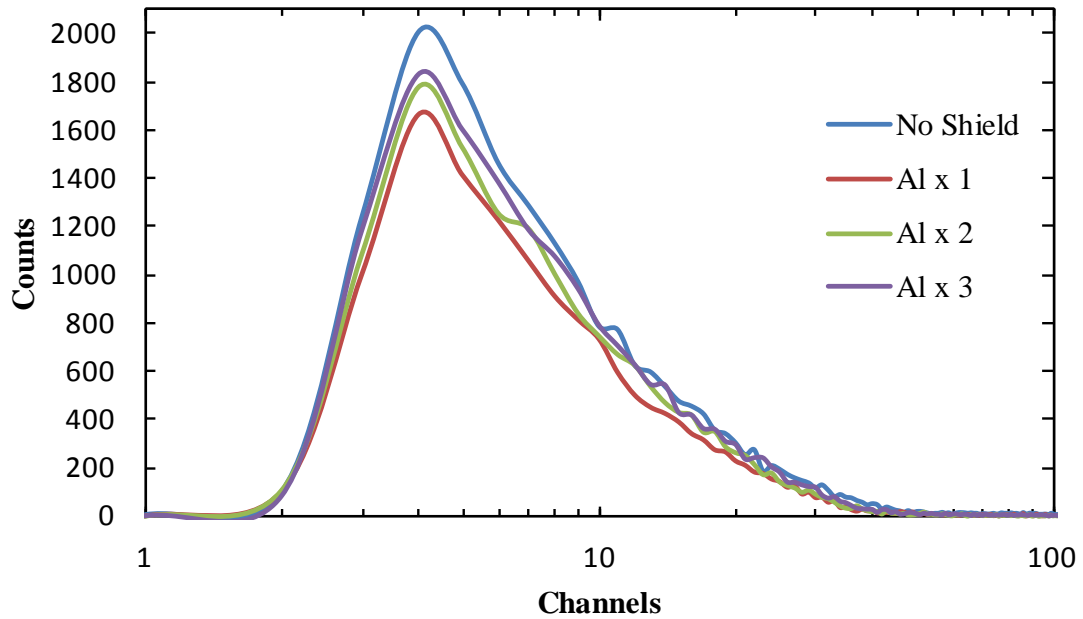


Figure 19: No shielding versus layers of aluminum on 17 December. The blue line is the result from no shielding, the red line is the result with one layer of aluminum shielding, the green line is the result of two layers of shielding, and the purple line is the result of three layers of shielding.

Table 3: No shielding versus layers of aluminum on 17 December.

Material	Total Counts	Percent Change Versus No Shielding
No Shield	18727 +/- 136.85	
Al x 1	14906 +/- 122.09	20.40 +/- 0.87
Al x 2	16359 +/- 127.90	12.64 +/- 0.93
Al x 3	17459 +/- 132.13	6.77 +/- 0.98

5.1.2 Sample X_{woB} Shielding with TEPC

Figure 20 shows the TEPC with no shielding material against one, two and three layers of shielding with sample X_{woB} . The most noticeable result shown in this plot, which was observed in all experimental days, was that using the three layers of sample X_{woB} shielding and the one layer of sample X_{woB} shielding were extremely close and at times overlapped in their error. Table 4 shows the tabulated data that coincide with Figure 20. The summations of the counts under each curve were taken per experiment and Equation 5.1 and 5.3 were applied to give a percentage difference in shielding material.

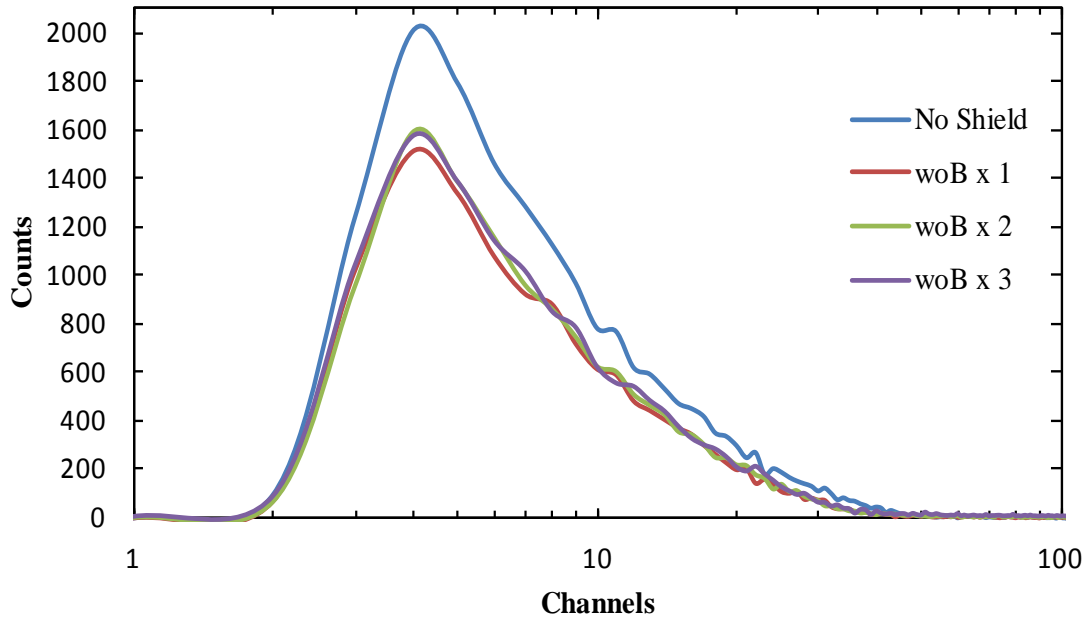


Figure 20: No shielding versus layers of sample X_{woB} on 17 December. The blue line is the result from no shielding, the purple line is the result with three layers of sample X_{woB} shielding, the green line is the result of two layers of sample X_{woB} shielding, and the red line is the result of one layer of sample X_{woB} shielding.

Table 4: No shielding versus layers of sample X_{woB} on 17 December.

Material	Total Counts	Percent Change Versus No Shielding
No Shield	18727 +/-136.85	
woB x 1	13737 +/-117.20	26.65 +/- 0.82
woB x 2	14043 +/- 118.50	25.01 +/- 0.84
woB x 3	14243 +/-119.34	23.94 +/- 0.85

5.1.3 Sample X_{wB} Shielding with TEPC

Figure 21 shows the TEPC with no shielding material against one, two, and three layers of sample X_{wB} . The most noticeable result shown in this plot, which was observed for all experiments, was that three layers of sample X_{wB} consistently performed better than two layers of shielding. Subsequently, two layers of shielding material functioned better than one layer of shielding material. Table 5 shows the tabulated data that coincide

with Figure 21. It should be noted that on 17 December, the results for three layers of shielding and two layers of shielding were almost identical. Unexpectedly, the results were not confirmed by later experiments. There were clear statistical differences between the three different layers of sample X_{wB} .

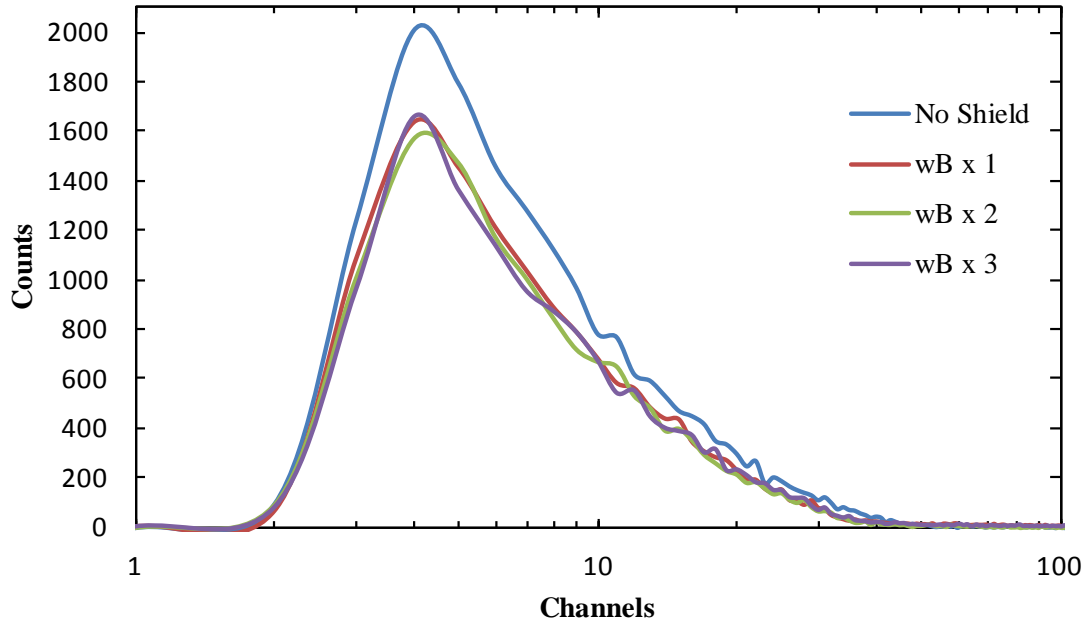


Figure 21: No shielding versus layers of sample X_{wB} on 17 December. The blue line is the result from no shielding, the purple line is the result with three layers of sample X_{wB} shielding, the green line is the result of two layers of sample X_{wB} shielding, and the red line is the result of one layer of sample X_{wB} shielding.

Table 5: No shielding versus varying layers of sample X_{wB} on 17 December.

Material	Total Counts	Percent Change Versus No Shielding
No Shield	18727 +/- 136.85	
wB x 1	14796 +/- 121.64	20.99 +/- 0.87
wB x 2	14401 +/- 120.00	23.10 +/- 0.85
wB x 3	14363 +/- 119.85	23.30 +/- 0.85

5.1.4 TEPC versus One Layer of Shielding

Using the data from all TEPC tests, three different types of shields in the one layer configuration were compared to the TEPC with no shield. Figure 23 shows the results without normalizing for density and thickness of the shielding materials. Table 6 gives the calculated percentage better than with no shielding and the calculated percentage better than one layer of aluminum shielding using Equation 5.1 and 5.3. Table 6 also shows the results after normalizing the density and thickness to T6061 for comparison. The most significant result from this data is that sample X_{woB} performed better than the other materials when evaluated against the calculated percentage better than no shielding and the calculated percentage better than only one layer of aluminum shielding. This observation was consistent in all experiments.

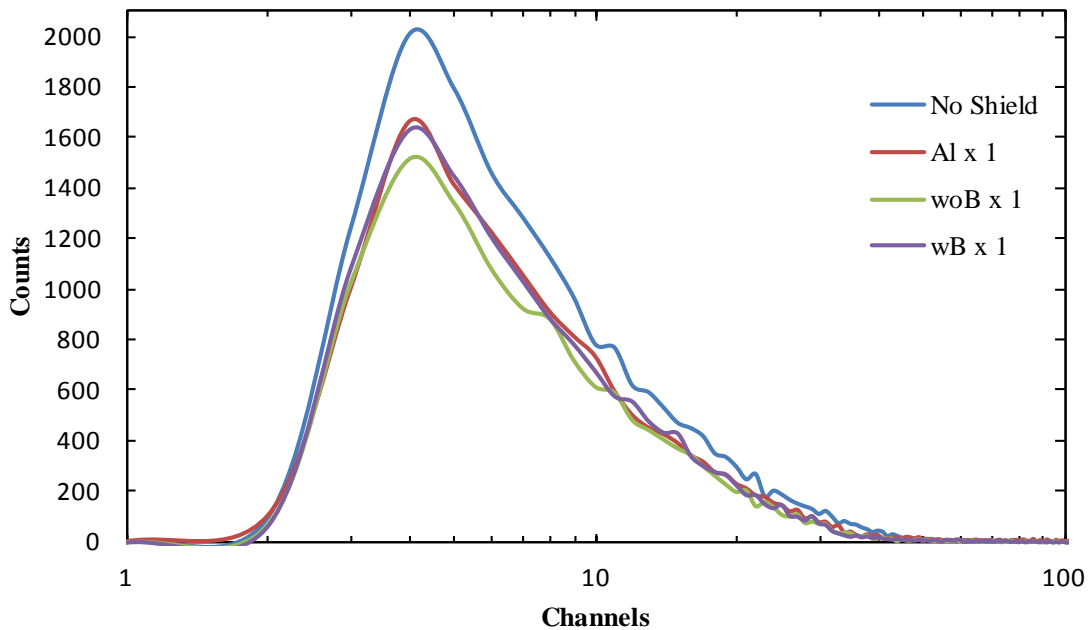


Figure 22: No shielding versus one layer of shielding material on 17 December. The blue line is the result from no shielding, the purple line is the result with one layer of sample X_{wB} shielding, the green

line is the result with one layer of sample X_{woB} shielding, and red line is the result of one layer of T6061 shielding.

Table 6: No shielding versus one layer of shielding material on 17 December.

Material	Total Counts	Percentage Change Versus No Shielding	Percent Change Versus Al x 1	Correcting for Density and Thickness Versus Al x 1
No Shield	18727 +/- 136.85			
Al x 1	14906 +/- 122.09	20.40 +/- 0.87		
woB x 1	13737 +/- 117.20	26.65 +/- 0.82	7.84 +/- 1.09	50.72 +/- 0.70
wB x 1	14796 +/- 121.64	20.99 +/- 0.87	0.74 +/- 1.15	16.04 +/- 1.02

5.1.5 TEPC versus Two Layers of Shielding

Using the data from all the TEPC experiments, the three different types of shielding for the two layered configuration were compared to the TEPC with no shielding. Figure 23 shows the results of this analysis without normalizing for density and thickness of the shielding materials, and Table 7 gives the calculated percentage better than no shielding and the calculated percentage better than two layers of aluminum shielding using Equation 5.1 and 5.3. Table 7 also shows the results after normalizing the density and thickness to T6061 for comparison. The most notable result identified was that sample X_{woB} performed better than the other shields when evaluating them against the calculated percentage better than no shielding and the calculated percentage better than two layers of aluminum. This observation was consistent in all experiments.

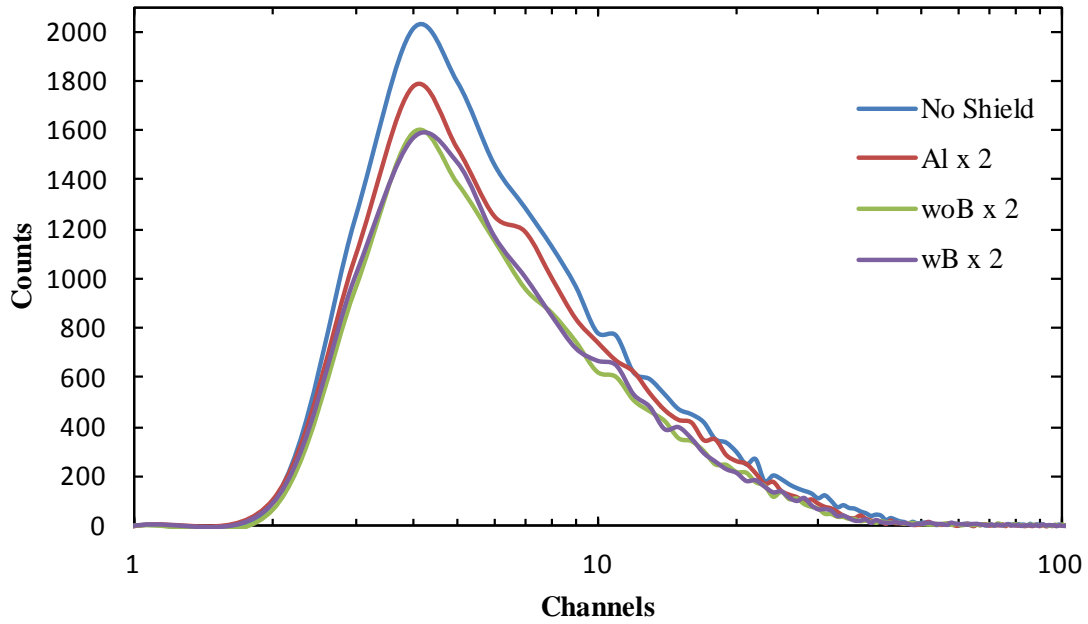


Figure 23: No shielding versus two layers of shielding material on 17 December. The blue line is the result from no shielding, the purple line is the result with two layers of sample X_{wB} shielding, the green line is the result with two layers of sample X_{woB} shielding, and red line is the result of two layers of T6061 shielding.

Table 7: No shielding versus two layers of shielding material on 17 December.

Material	Total Counts	Percentage Change Versus No Shielding	Percent Change Versus Al x 2	Correcting for Density and Thickness Versus Al x 2
No Shield	18727 +/- 136.85			
Al x 2	16359 +/- 127.90	12.64 +/- 0.93		
woB x 2	14043 +/- 118.50	25.01 +/- 0.84	14.16 +/- 0.99	54.10 +/- 0.64
wB x 2	14401 +/- 120.00	23.10 +/- 0.85	11.97 +/- 1.06	25.54 +/- 0.89

5.1.6 TEPC versus Three Layers of Shielding

Using the data from all the TEPC runs, the three different types of shields for the three layered configurations were compared to the TEPC with no shielding. Figure 24 shows the results of this analysis without normalizing for density and thickness of the

shielding materials, and Table 8 gives the calculated percentage better than no shielding and the calculated percentage better than three layers of aluminum shielding using Equation 5.1 and 5.3. Table 8 also shows the results after normalizing the density and thickness to T6061 for comparison. The most significant result from this data was that sample X_{woB} shielded the TEPC better than sample X_{wB} on every test, with the exception of the experiment conducted on 19 December. The summation of the counts for both sample X_{woB} and sample X_{wB} for each experiment falls within each sample's standard deviation.

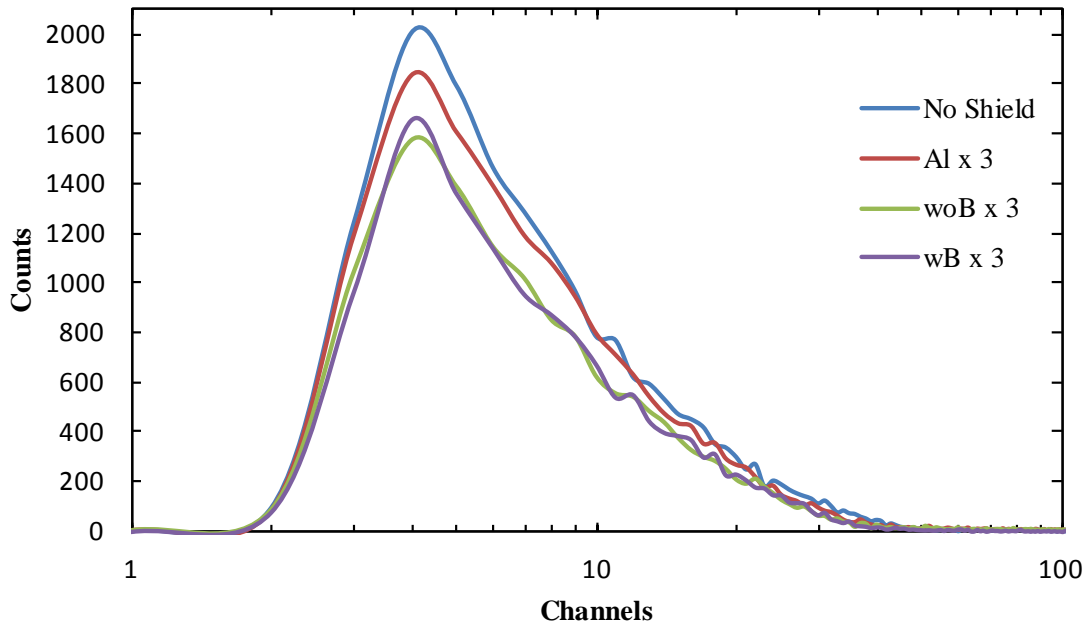


Figure 24: No shielding versus three layers of shielding material on 17 December. The blue line is the result from no shielding, the purple line is the result with three layers of sample X_{wB} shielding, the green line is the result with three layers of sample X_{woB} shielding, and the red line is the result of three layers of T6061 shielding.

Table 8: No shielding versus three layers of shielding material on 17 December.

Material	Total Counts	Percentage Change Versus No Shielding	Percent Change Versus Al x 3	Correcting for Density and Thickness Versus Al x 3
No Shield	18727 +/- 136.85			
Al x 3	17459 +/- 132.13	6.77 +/- 0.98		
woB x 3	14243 +/- 119.34	23.94 +/- 0.85	18.42 +/- 0.92	56.38 +/- 0.60
wB x 3	14363 +/- 119.85	23.30 +/- 0.85	17.73 +/- 0.93	30.41 +/- 0.82

5.1.7 Summary of TEPC Experiment

By plotting all the data recorded from the TEPC experiments, trends with the shielding material became very prominent. The data of the total counts can be seen in Tables 9 through 11. By normalizing the thicknesses and the densities and plotting the total counts the TEPC detected per type of shielding material as in Figure 25 trends emerge.

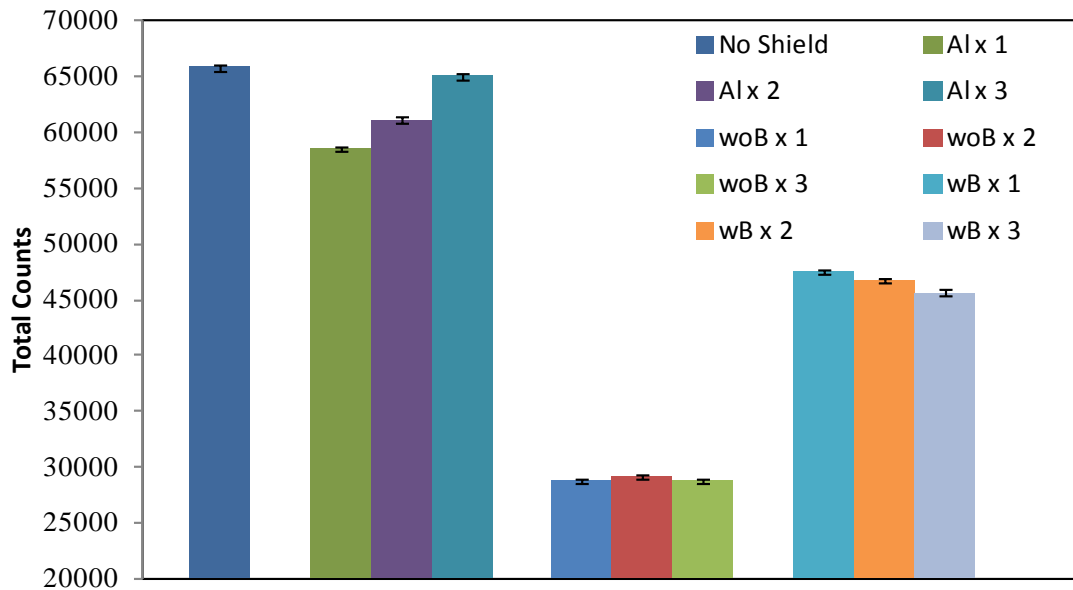


Figure 25: Histogram plot of the total counts per shielding type. By plotting the total counts detected by the TEPC over all four days, trends are seen in different types of shielding materials. The legend gives a detailed color coded breakdown of the material and layered configuration. The error bars are the standard deviation of the total counts per shielding type.

In Figure 25, the highest number of counts was recorded with the TEPC with no shield, yet what unexpectedly occurred was that the three layers of aluminum shield recorded the next highest number of counts. This result was not anticipated because it was believed that the more material placed in front of the TEPC, the less neutron counts the TEPC would record. What occurred with the aluminum was that additional shielding layers in front of and surrounding the TEPC resulted in a larger area for the neutron to come into contact with the aluminum, allowing some of the neutrons to scatter off the aluminum, which subsequently interacted with the active volume of the TEPC and were detected. The detectable neutrons decreased when two layers of aluminum were used, and then further decreased when one layer of aluminum was used. Aluminum with one layer shielded 11.07% of the neutrons compared to no shielding. Aluminum with two

layers shielded 7.19% of the neutrons compared to no shielding. Aluminum with three layers shielded 1.18% of the neutrons compared to no shielding. Overall, aluminum, when used as a shielding material, proved to be inferior to all the materials tested when a comparison of each was made to the TEPC with no shielding material.

Results of sample X_{woB} , when used as a shielding material, can be found in Figure 25. The total counts using one, two and three layers of sample X_{woB} did not follow the same pattern as for the aluminum. Testing one layer and three layers of sample X_{woB} in front of the TEPC performed statistically identical when all the counts were added for the four experimental days. Also, each daily test using one and three layers of sample X_{woB} found that the counts were statistically identical. A finding that proved noteworthy was that two layers of shielding with sample X_{woB} recorded slightly higher count than one layer or three layers of sample X_{woB} . It is hypothesized the reason why the three layers of sample X_{woB} did not have the most counts was because this shielding material has a greater ability to down-scatter the neutrons. By down-scattering the neutron with the three layers of material, the fast neutrons are slowed enough so the TEPC did not record any slower neutron interactions.

Results of sample X_{wB} as the shielding material can also be found in Figure 25. The total counts with one, two and three layers of sample X_{wB} decreases as the thickness of the layers increases. When testing sample X_{wB} , the thicker the shielding material, the more captures that occur, which results in lower counts on the TEPC.

When evaluating aluminum and the composites in a fast neutron environment, aluminum will, in theory and modeling, allow the most neutrons to pass through the material, and that was confirmed using the TEPC. When testing the composite materials

in a fast neutron rich environment, sample X_{woB} consistently had a lower neutron count when compared to sample X_{wB} .

Table 9: Summary of TEPC data for no shielding and one layer of shielding

Material	Sum Counts	Percentage Change Versus No Shielding	Percentage Change Versus Al x 1	Correcting for Density and Thickness Versus Al x 1
No Shield	65828 +/- 256.57			
Al x 1	58544 +/- 241.96	11.07 +/- 0.51		
woB x 1	53869 +/- 232.10	18.17 +/- 0.48	7.99 +/- 0.55	50.80 +/- 0.35
wB x 1	56155 +/- 236.97	14.69 +/- 0.49	4.08 +/- 0.57	18.87 +/- 0.50

Table 10: Summary of TEPC data for no shielding and two layers of shielding

Material	Sum Counts	Percentage Change Versus No Shielding	Percentage Change Versus Al x 2	Correcting for Density and Thickness Versus Al x 2
No Shield	65828 +/- 256.57			
Al x 2	61095 +/- 247.17	7.19 +/- 0.52		
woB x 2	54488 +/- 233.43	17.23 +/- 0.48	10.81 +/- 0.53	52.31 +/- 0.34
wB x 2	55280 +/- 235.12	16.02 +/- 0.48	9.52 +/- 0.53	23.46 +/- 0.47

Table 11: Summary of TEPC data for no shielding and three layers of shielding

Material	Sum Counts	Percentage Change Versus No Shielding	Percentage Change Versus Al x 3	Correcting for Density and Thickness Versus Al x 3
No Shield	65828 +/- 256.57			
Al x 3	65054 +/- 255.06	1.18 +/- 0.54		
woB x 3	53828 +/- 232.01	18.23 +/- 0.48	17.26 +/- 0.48	55.76 +/- 0.31
wB x 3	53987 +/- 232.35	17.99 +/- 0.48	17.01 +/- 0.48	29.8 +/- 0.43

5.2 Foil Activation Experiment

Counting for these experiments was conducted using the HPGe detectors in building 470 and in building 194. The plots in this section are overlaid on each figure to

categorize the differences found in each foil activation experiment. Background readings for each detector were taken on 17 December for the exact counting time the activated foils were placed in the HPGe detectors.

5.2.1 Foil Activation with Indium Foils

The indium foil spectrum counts are shown in Figure 26 after the background readings were removed. Figure 26 presents all four experimental runs that were conducted using the indium foils. In the full spectrum plot of indium, the weights of the foils, different densities and thickness for the shielding materials were not normalized; it only shows the results from the HPGe detector.

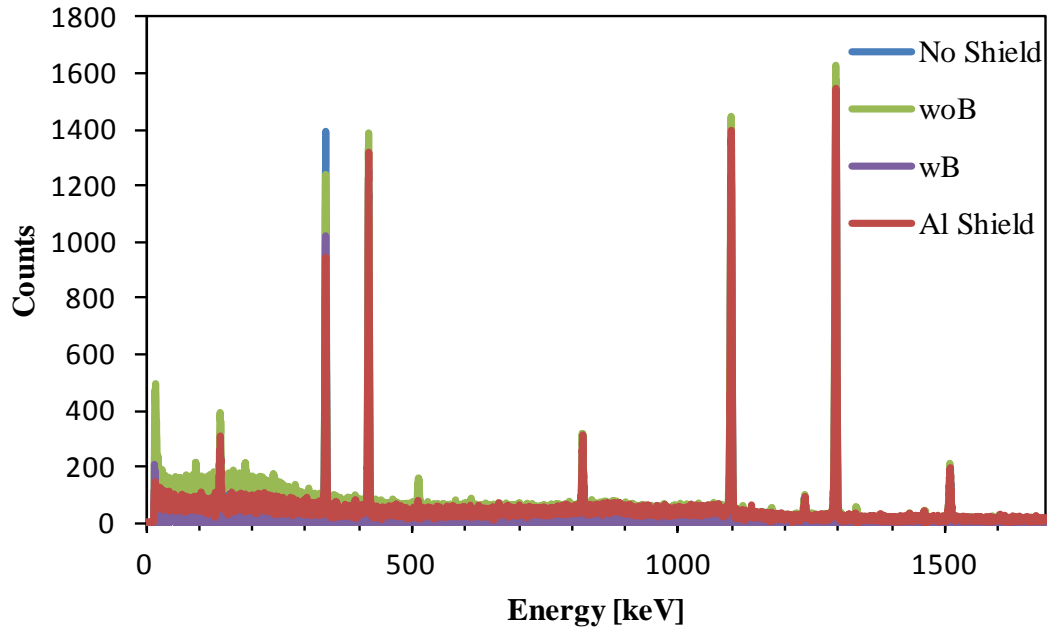


Figure 26: Foil activation spectrum of indium after subtracting the background spectrum. This figure shows the results of four separate foil activation experiments. All experiments used the PuBe source to activate the indium foil. The blue spectrum is the result of the foil with no shielding. The green spectrum is the result of the foil with sample X_{woB} shielding. The purple spectrum is the result of the foil with sample X_{wB} . The red spectrum is the result of the foil with aluminum shielding.

Figure 27 identifies indium's 336 keV peak, which has a threshold activation of 0.5 MeV. The counts that were recorded are significantly greater than were plotted in Figure 26 due to the fact that the weights of the foils were normalized to one gram and the density and thickness is normalized to aluminum. This accounts for a larger number of counts in the 336 keV peak in Figure 27 when compared to Figure 26. By applying Equation 5.1 and 5.3, the most notable observation from Figure 27 is that when evaluating the area under the peak, sample X_{wB} performed better in shielding 0.5 MeV and greater energy neutrons by 16% over aluminum, and sample X_{woB} performed better in shielding those neutrons by 37% over aluminum.

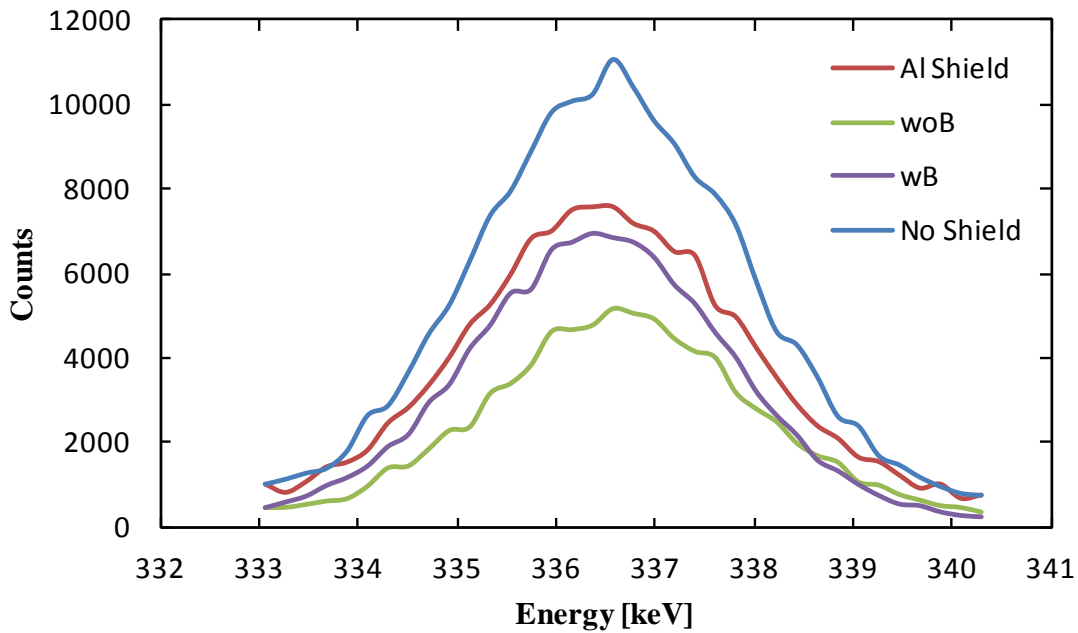


Figure 27: Foil activation spectrum of indium's 336 keV peak corrected for weight, density, and thickness. After subtracting the background spectrum, this is the final product of the 336 keV peak. This figure shows the results of four separate foil activation experiments. All experiments used the Pu-Be source to activate the indium foil. The blue spectrum is the result of the foil with no shielding. The green spectrum is the result of the foil with sample X_{woB} shielding. The purple spectrum is the result of the foil with sample X_{wB} . The red spectrum is the result of the foil with aluminum shielding.

Table 12 displays the results of applying Equation 5.1 and 5.3 that seek to address the primary objective of this thesis; do the composite materials shield neutrons better than aluminum? As show in Table 12 below, when evaluating the area under the 336 keV peak, sample X_{wB} provided 16.45 +/- 0.34 percent better shielding than aluminum, and sample X_{woB} provided 37.17 +/- 0.28 percent better shielding than aluminum. The difference in counts recorded for sample X_{woB} shows statistically that sample X_{woB} performs slightly better than aluminum and sample X_{wB} in shielding the neutrons from interacting with the nuclei.

Table 12: Summary data for indium's 336 keV peak after correcting for weight, density, and thickness

Percent Change Versus No Shielding			Percent Change Versus T6061 Shielding		
Material	Al Shield	woB Shield	wB Shield	woB Shield	wB Shield
Area	25.98 +/- 0.27	53.49 +/- 0.19	38.15 +/- 0.24	37.17 +/- 0.28	16.45 +/- 0.34
Peak	31.67 +/- 0.05	54.20 +/- 0.04	37.85 +/- 0.06	32.97 +/- 0.05	9.05 +/- 0.06

5.2.2 Foil Activation with Zinc Foils

The zinc foil spectrum, following the removal of the background reading, is shown in Figure 28. Four experimental tests were conducted using zinc foils in the full spectrum plot of zinc, the weights of the foils, different densities and thickness for the shielding materials were not normalized; it only shows the results from the HPGe detector.

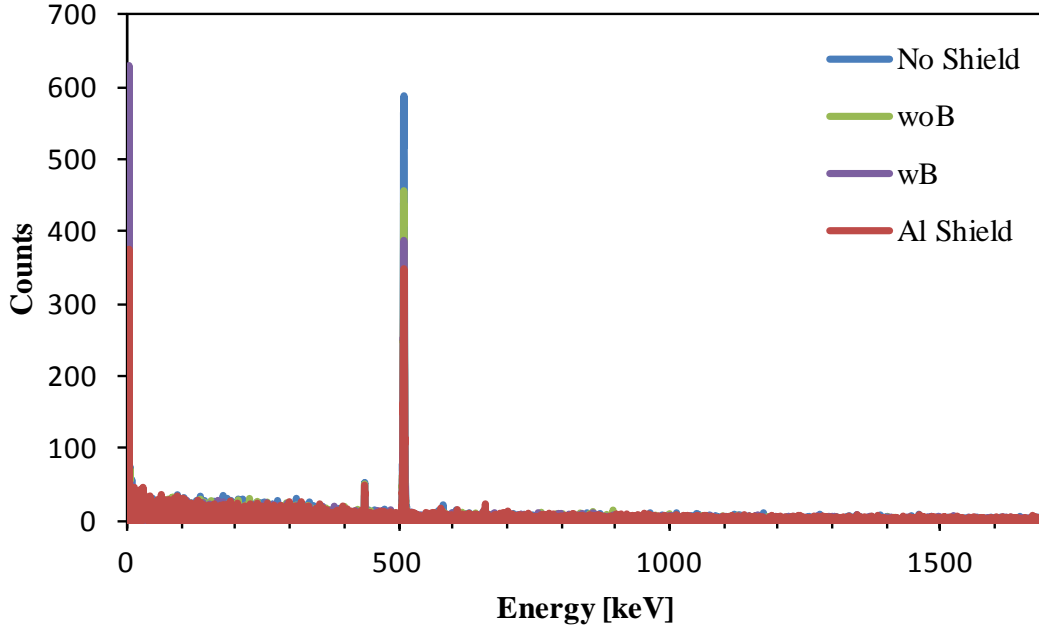


Figure 28: Foil activation spectrum of zinc after subtracting the background spectrum. This figure shows the results of four separate foil activation experiments. All experiments used the PuBe source to activate the zinc foil. The blue spectrum is the result of the foil with no shielding. The green spectrum is the result of the foil with sample X_{woB} shielding. The purple spectrum is the result of the foil with sample X_{wB} . The red spectrum is the result of the foil with aluminum shielding.

Figure 29 indicates zinc's 511 keV peak, which has a threshold activation of 2.0 MeV. The counts detected are significantly higher in Figure 28, because the foil weight is normalized to one gram and density and thickness is normalized to the aluminum sample to allow comparison of the different experiments. By applying Equation 5.1 and 5.3, the most notable observation from Figure 29 is that the sample X_{woB} reduced the peak counts more than aluminum and sample X_{wB} materials, when comparing them to no shielding. When evaluating the area under the peak, sample X_{woB} shielding reduced the peak more than aluminum and sample X_{wB} materials. Table 13 shows the results of applying Equation 5.1 and 5.3 when comparing shielding capabilities of composite materials to aluminum.

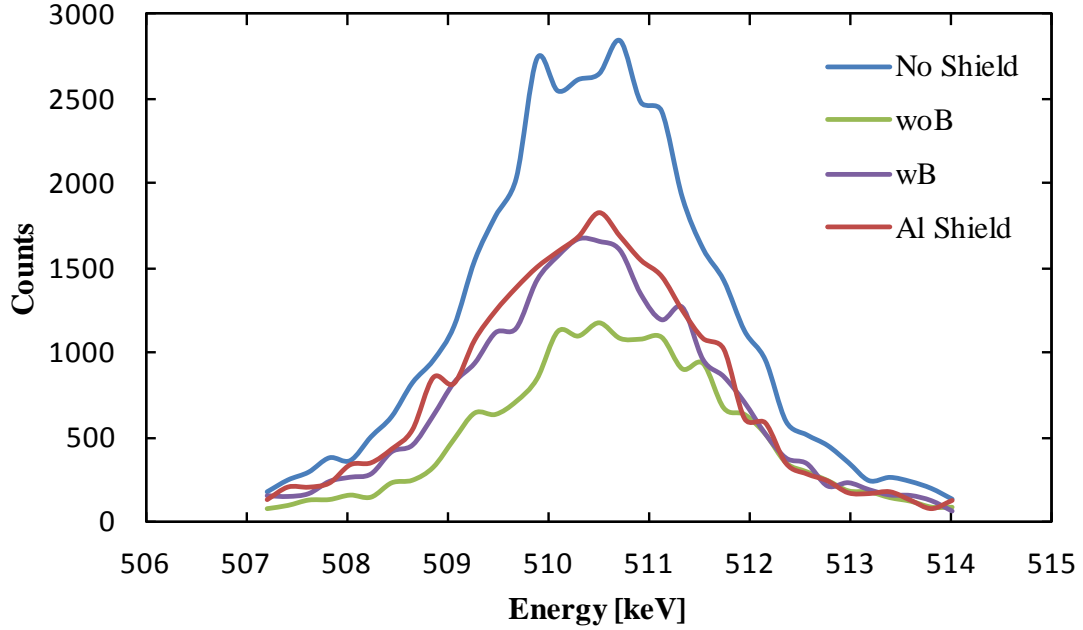


Figure 29: Foil activation spectrum of zinc’s 511 keV peak corrected for weight, density, and thickness, after subtracting the background spectrum. This figure shows the results of four separate foil activation experiments. All experiments used the Pu-Be source to activate the zinc foil. The blue spectrum is the result of the foil with no shielding. The green spectrum is the result of the foil with sample X_{woB} shielding. The purple spectrum is the result of the foil with sample X_{wB} . The red spectrum is the result of the foil with aluminum shielding.

As displayed in Table 13, when evaluating the area under the 511 keV peak, sample X_{woB} provides 35.69 ± 0.10 percent better shielding of neutrons of energy 2.0 MeV and above and sample X_{wB} provides 8.40 ± 0.12 percent better shielding of neutrons of energy 2.0 MeV and above than T6061 aluminum. The difference in counts recorded for sample X_{woB} shows statistically that sample X_{woB} performs better than aluminum and sample X_{wB} in shielding neutrons of energy 2.0 MeV and above as evinced by the results of counts under zinc’s 511 keV peak.

Table 13: Summary data for zinc's 511 keV peak after correcting for weight, density, and thickness

Percent Change against No Shielding				Percent Change against T6061 Shielding	
Material	Al Shield	woB Shield	wB Shield	woB Shield	wB Shield
Area	36.50 +/- 0.09	59.16 +/- 0.09	41.83 +/- 0.09	35.69 +/- 0.10	8.40 +/- 0.12
Peak	31.13 +/- 0.02	59.33 +/- 0.02	37.76 +/- 0.02	40.95 +/- 0.02	9.62 +/- 0.03

5.2.3 Foil Activation with Gold Foils

The gold foil gamma spectrum is shown in Figure 30. This graph presents the results after the background readings were removed, and it also displays the four experimental tests that were conducted using the gold foils. In the full spectrum plot of gold, different densities and thickness for the shielding materials were not normalized; it only shows the results from the HPGe detector.

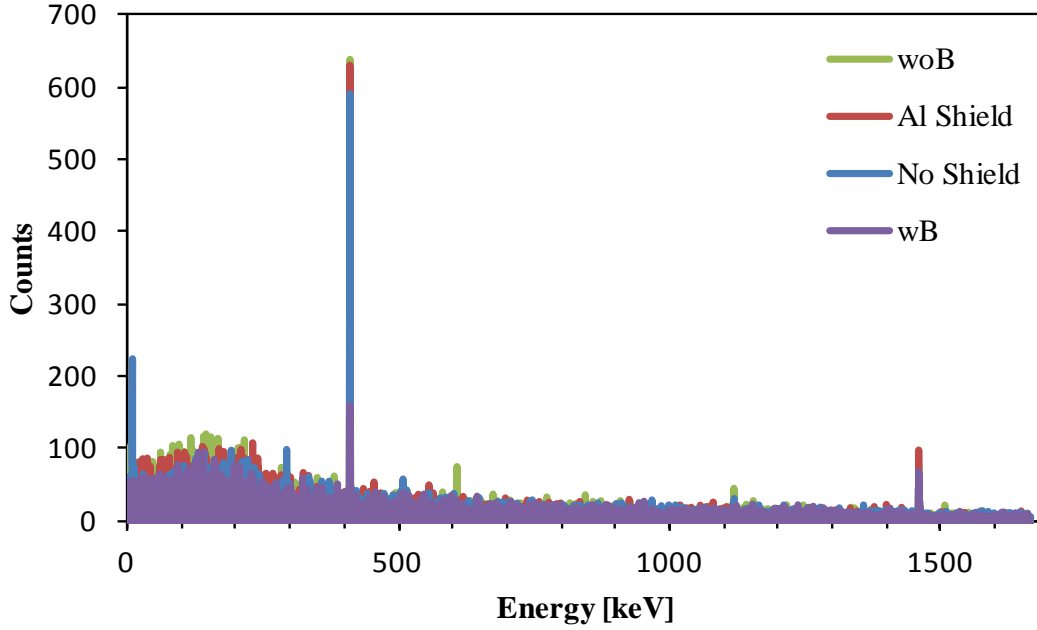


Figure 30: Foil activation spectrum of gold after subtracting the background spectrum. This figure shows the results of four separate foil activation experiments. All experiments used the PuBe source to activate the gold foil. The blue spectrum is the result of the foil with no shielding. The green spectrum is the result of the foil with sample X_{woB} shielding. The purple spectrum is the result of the foil with sample X_{wB} . The red spectrum is the result of the foil with aluminum shielding.

In Figure 31, gold's 411 keV thermal activation peak is plotted. The counts identified in Figure 31 are significantly higher than those shown in Figure 30, because the foil weight is normalized to one gram and density and thickness is normalized to the aluminum sample to allow comparison of the different experiments. By applying Equation 5.1 and 5.3, the most notable observation from Figure 31 is the significant reduction in thermal neutrons that activated the gold foil when sample X_{wB} was used as the shielding material. Another notable result was an increase in gold foil activation due to down-scattering of fast neutrons; this increased the neutron's probability to be captured by the gold foil, resulting in more counts. Table 14 shows the results of applying

Equation 5.1 and 5.3 when determining whether composite materials shield neutrons better than aluminum.

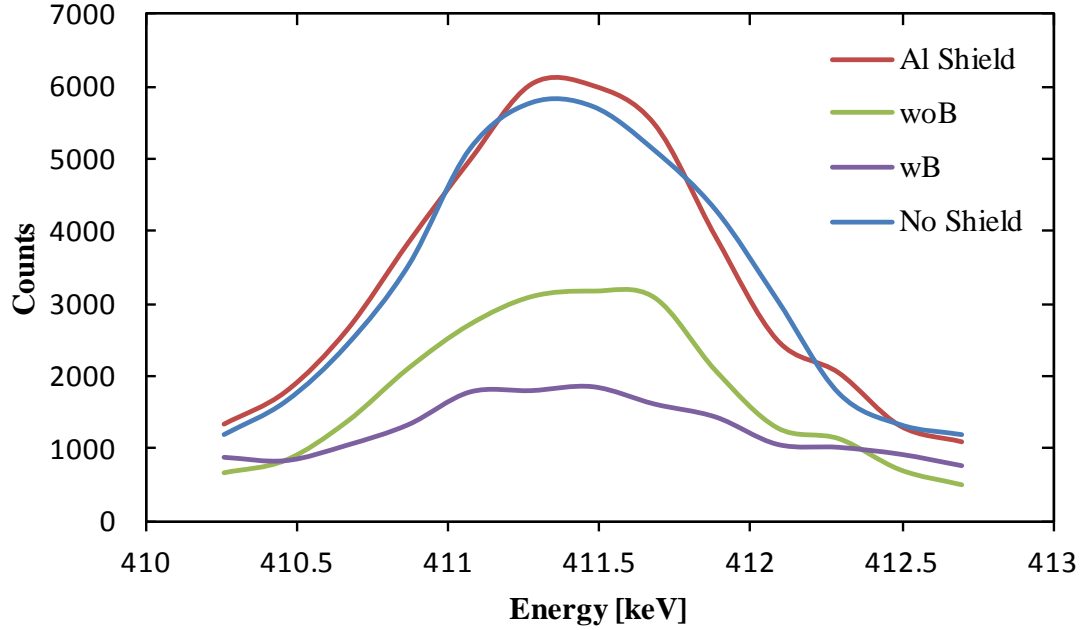


Figure 31: Foil activation spectrum of gold's 411 keV peak corrected for weight, density, and thickness after subtracting the background spectrum. This figure shows the results of four separate foil activation experiments. All experiments used the Pu-Be source to activate the gold foil. The blue spectrum is the result of the foil with no shielding. The green spectrum is the result of the foil with sample X_{woB} shielding. The purple spectrum is the result of the foil with sample X_{wB} . The red spectrum is the result of the foil with aluminum shielding.

Table 14: Summary data for gold's 411 keV peak after correcting for weight, density, and thickness

Material	Percent Change against No Shielding			Percent Change against T6061 Shielding	
	Al Shield	woB Shield	wB Shield	woB Shield	wB Shield
Area	-1.62 +/- 0.13	46.08 +/- 0.09	61.11 +/- 0.07	46.95 +/- 0.12	61.73 +/- 0.10
Peak	-4.80 +/- 0.04	44.42 +/- 0.03	67.51 +/- 0.02	46.97 +/- 0.04	69.00 +/- 0.03

5.2.4 Summary of Foil Activation Experiment

After normalizing the densities and the thickness to T6061, both composites reduced the activation of the foils. When using fast foil activation the sample without

boron performs better at reducing the activation of indium and zinc. When using thermal foil activation the sample with boron performs better at reducing the activation of the thermal neutrons.

Upon reviewing the data collected from the foil activation experiments, several observations can be made. The most significant result from the foil activation experiments was observed when using the gold foils. Sample X_{wB} significantly reduced the thermal neutrons due to absorption in the boron by more than 60% when compared to T6061 shielding or no shielding. As seen in both the theory and modeling sections, when boron was included in the composite material, thermal neutrons were significantly reduced. Another relevant finding, because it ties into the primary objective to this thesis, found that sample X_{woB} after normalizing the thickness and density to T6061 shields fast neutrons better than aluminum and sample X_{wB} . The indium foil activation results show that sample X_{woB} shields fast neutrons above 0.5 MeV, 37% more efficiently than T6061 when considering the area under the peak. Also after normalizing the thickness and density to T6061, sample X_{woB} shielded fast neutrons 35% more than aluminum when considering the area under zinc's 511 keV peak.

CHAPTER 6

CONCLUSION

6.1 Summary of Findings

The first part of the primary objective for this research was to develop a MCNP model and compare the neutron flux through aluminum and composite materials to determine the relative neutron shielding effectiveness of these materials. This was accomplished by writing and running an MCNP simulation (Appendix A); there was a difference between the flux that passed through the three different types of shielding materials. The results of the modeling did not match very closely to the TEPC experimental observations for a variety of reasons. The model dealt with the flux passing through the different materials, and the TEPC results recorded the recoil proton spectrum from the PuBe source. The foil activation experiment recorded the gamma rays emitted by the foils and collected by the HPGe detector. The percentage of neutrons transmitted in the model after normalizing the materials for thickness and density gave similar percentages to the normalized percentages of the shielded foil activation experiments. Also, the models were all based on AFIT's 2.45 MeV D+D generator, and because of the generator breakdown, the experiments were modified to use the PuBe source. Unlike the generator, which emits a mono-energetic source of neutrons, the PuBe source produces a spectrum of neutrons ranging from 0.5 to 10 MeV in energy.

The second part of the primary objective for this research was to use a Tissue Equivalent Proportional Counter (TEPC) to develop a method to measure the relative differences between the amount of neutrons that passed through each shielding material

and are still detectable. A five-sided box was constructed of each type of shielding material, and the sixth side of the box was removed to allow the TEPC to be inserted into the shielding material. Each box had three layers of shielding material on five sides of the box. Each time an experiment concluded, one layer of shielding material was removed from the five sides of the box. During each test, the TEPC recorded recoil proton spectrum of the PuBe source. The results revealed that aluminum was the least effective at shielding the TEPC from neutrons. After normalizing the density and thickness of the composites to T6061, sample X_{woB} performed better at shielding neutrons from the TEPC than sample X_{wB} .

The third part of the primary objective for this study was to use the neutron generator at AFIT to conduct fast foil activation experiments to determine the relative difference in the amount of neutrons shielded by the materials. This objective was modified when the neutron generator broke, so the foil activation experiment was changed to use the Pu-Be source. After normalizing the density and thickness of the composites to T6061, the outcome of these experiments demonstrated that sample X_{woB} shielded fast neutrons better than either T6061 or sample X_{wB} , but sample X_{wB} shielded thermal neutrons approximately 62% better than aluminum, whereas X_{woB} shielded 47% better than aluminum.

When comparing the modeling results to the TEPC results and foil activation results, in the MCNP model with aluminum shielding provided the worst shielding of all the materials tested, and that result was also confirmed in the TEPC experiments. When examining the results from the MCNP model with sample X_{woB} as the shielding material, it would be expected from the modeling results that sample X_{woB} would provide a middle

ground of shielding between aluminum and sample X_{wB} , but that was not the case. Sample X_{woB} performed the best of all the materials in shielding neutrons in the TEPC experiments and in the fast foil activation experiments. When examining the results from the MCNP model with sample X_{wB} as the shielding material, it would be expected from the modeling results that it would provide the best shielding against neutrons, but that was not the case all of the time. Most of the time, sample X_{wB} performed slightly worse than sample X_{woB} . As shown in simulations and in the foil activation experiments, sample X_{wB} provided the best shielding against thermal neutrons because of boron's high cross section for capturing them.

The secondary objective was to ensure the density of the composite materials was equal to or less than the tested aluminum. The secondary objective was accomplished by simply weighing all the materials and measuring the materials to verify their densities. A scale, with accuracy up to a thousandth of a gram, was used to determine the measured density of the materials, and a digital micrometer was used to measure the volume of the sample. A density of 2.40 grams/cm^3 was calculated for sample X_{wB} , a density of 1.77 grams/cm^3 was calculated for sample X_{woB} , and a density of 2.66 grams/cm^3 was calculated for the aluminum tested. The secondary objective was completed and confirmed, demonstrating that the composite materials were lighter in density than aluminum.

6.2 Future Work

Composites have great potential when used as a shield against thermal neutrons, but this was not the key objective of the study. The objective was to find a substance that would shield against fast neutrons.

Based upon the research conducted, the following are recommendation for future work on the composite material. First, develop a GEANT modeling simulation that would include the detector to be used in the experimental section. Ensure AFIT's neutron generator is operational, because the optimal method of evaluating experimental results is with a mono-energetic source of neutrons that can be modeled in a simulation, and this source can only be provided by a neutron generator. Relocate AFIT's neutron generator to the basement of building 470. Moving the generator will allow trained students to operate the neutron generator with less impact on other students and faculty with the two-person rule in effect. Modify the composite material slightly to incorporate additional hydrogen into the material. This could be accomplished by adding several hydrogenated carbon fibers, or by adding a polyethylene mixture into the composite material. Proper bonding and structural limits would need to be calculated. Ensure the material thicknesses are the same. Other questions that were unanswered in the research were the strength of the composite material when compared to aluminum. How do these composite materials compare to aluminum in high electron radiation environments, high x-ray environments, and in high gamma ray environments. These questions could be the topic of another study.

APPENDIX A – Simulation Codes

T6061

```

Title
1      1      -2.66295      1 -2 3 -4 -5 6      imp:n 1      $ Material,Density 2.7
10     0      -1 -100      imp:n 1      $ Vacuum
11     0      2 -100      imp:n 1      $ Vacuum
12     0      (1:-2:-3:5) -100      imp:n 0      $ kill particle
13     0      (1:-2:4:-6) -100      imp:n 0      $ kill particle
100    0      100      imp:n 0      $ Outside universe

1 py 0.1      $ Front side of the material
2 py 2.64      $ Back side of the material
3 px -99.96      $ left side of the material
4 px 99.96      $ right side of the material
5 pz 99.96      $ top side of the material
6 pz -99.96      $ bottom side of the material
100 so 100      $ universe

mode n
m1 13027.70c -0.9729 22000 -0.0015 30000 -0.0025 24000 -0.0035 12000 -0.012 &
25055.70c -0.0015 29000 -0.0040 26000 -0.007 14000 -0.008 $ T6061 Aluminium
sdef pos= 0 0 0 AXS= 0 1 0 VEC= 0 1 0 X=d1 Y=0 Z=d2 PAR=1 DIR=1 erg=2.45
SI1 -0.5 0.5 $ sampling range in the Xmin to Xmax
SP1 0 1      $ weighting for x sampling: here constant
SI2 -0.5 0.5 $ sampling range in the Ymin to Ymax
SP2 0 1      $ weighting for z sampling: here constant
NPS 1E7
c Tally
f2:n 2
e2 1E-9 1000ilog 2.45

```

sample X_{woB}

```

Title
1      1      -1.76737      1 -2 3 -4 -5 6      imp:n 1      $ Material , Density
10     0      -1 -100      imp:n 1      $ Vacuum
11     0      2 -100      imp:n 1      $ Vacuum
12     0      (1:-2:-3:5) -100      imp:n 0      $ kill particle
13     0      (1:-2:4:-6) -100      imp:n 0      $ kill particle
100    0      100      imp:n 0      $ Outside universe

1 py 0.1      $ Front side of the material
2 py 1.2125      $ Back side of the material
3 px -99.96      $ left side of the material
4 px 99.96      $ right side of the material
5 pz 99.96      $ top side of the material
6 pz -99.96      $ bottom side of the material
100 so 100      $ universe

mode n
m1 06000.70c -0.2600 28058.64c -0.3121 74184.65c -0.3343 &
08016.70c -0.05989 &
01001.70c -0.0226 07014.70c -0.0077 16032.70c -0.0077$ made up Carbon Material
sdef pos= 0 0 0 AXS= 0 1 0 VEC= 0 1 0 X=d1 Y=0 Z=d2 PAR=1 DIR=1 erg=2.45
SI1 -0.5 0.5 $ sampling range in the Xmin to Xmax
SP1 0 1      $ weighting for x sampling: here constant
SI2 -0.5 0.5 $ sampling range in the Ymin to Ymax
SP2 0 1      $ weighting for z sampling: here constant
NPS 1E7
c Tally
f2:n 2
e2 1E-9 1000ilog 2.45

```

sample X_{wB}

```

Title
1      1      -2.40191      1 -2 3 -4 -5 6      imp:n 1      $ Material , Density
10     0      -1 -100      imp:n 1      $ Vacuum
11     0      2 -100      imp:n 1      $ Vacuum
12     0      (1:-2:-3:5) -100      imp:n 0      $ kill particle
13     0      (1:-2:4:-6) -100      imp:n 0      $ kill particle
100    0      100      imp:n 0      $ Outside universe

1 py 0.1      $ Front side of the material
2 py 2.64      $ Back side of the material
3 px -99.96      $ left side of the material
4 px 99.96      $ right side of the material
5 pz 99.96      $ top side of the material
6 pz -99.96      $ bottom side of the material
100 so 100      $ universe

mode n
m1 06000.70c -0.2585 28058.64c -0.1979 74184.65c -0.2119 &
05011.70c -0.2039 05010.70c -0.0507 08016.70c -0.0464 &
01001.70c -0.0148 07014.70c -0.0072 16032.70c -0.0072$ made up Carbon Material
sdef pos= 0 0 0 AXS= 0 1 0 VEC= 0 1 0 X=d1 Y=0 Z=d2 PAR=1 DIR=1 erg=2.45
SI1 -0.5 0.5 $ sampling range in the Xmin to Xmax
SP1 0 1      $ weighting for x sampling: here constant
SI2 -0.5 0.5 $ sampling range in the Ymin to Ymax
SP2 0 1      $ weighting for z sampling: here constant
NPS 1E7
c Tally
f2:n 2
e2 1E-9 1000ilog 2.45

```

APPENDIX B – Filling the LET Detector

Appendix B gives detailed instructions on how to fill the ½ inch LET Detector [14, 15]. Most of the filling procedures were provided to me from Far West, the company that manufactures the detector and the gas filling system (GFS-1). I transposed most of the procedure provided by Far West into this appendix, but modified parts of it to actually account for my procedures for filling the detector. Figure 33 shows how to connect the vacuum pump, LET Detector, and fill gas to the GFS-1.

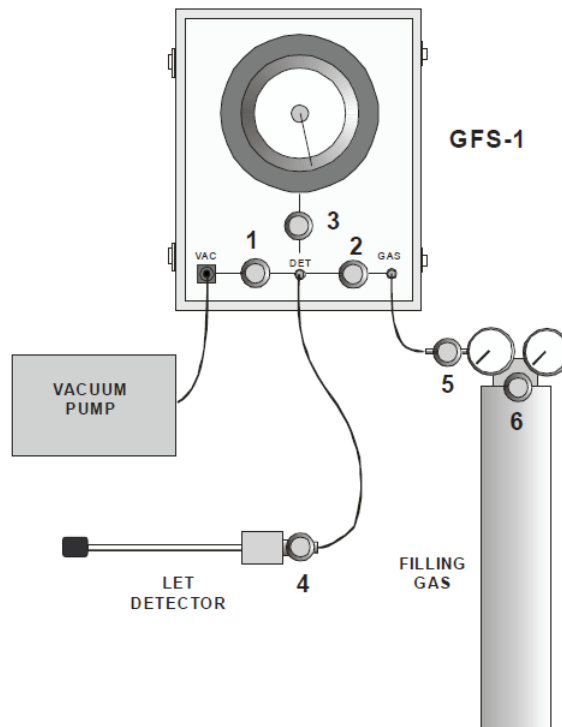


Figure 32: Gas Filling System 1 from Far West. Valves 1 through 6 are shown in this figure to ensure that proper identification of valves is known.

System Steps

1. Make sure valve 5 and 6 on the filling gas are closed.
2. Turn down the pressure on the regulator as far as it will go.
3. Open the tank valve #6 and also valve #5.
4. Slowly increase the regulator until the exit gauge reads a few PSI. You want the regulator to have some pressure but not very much. You will be filling the detector below

atmospheric pressure so any reading on the gauge will be enough. If it is set too high, it will be difficult to control the amount of gas when you fill the detector.

5. Close valves 5 and 6.

Now connect the system together.

1. Connect the vacuum pump to the hose barb on the GFS-1 using ½ to ¾ inch vacuum hose.
2. Connect the supply of filling gas to the port marked GAS on the GFS-1.
3. Make sure the valve to the detector #4 is closed, then connect the detector to the port marked DET on the GFS-1.

Startup/Evacuation

The lines need to be evacuated before you can fill the detector. The desire is to open all of the sections of the system and let them pump down. This way you know that each line is free of air. This step often takes several minutes.

1. Make sure the gauge valve #3 is closed. This protects the gauge.
2. Make sure valve to the detector #4 is closed. This protects the detector.
3. Make sure the valve to the filling gas #5 is closed. This isolates the filling gas.
4. Make sure the valve to the tank of filling gas #6 is closed.
5. Turn on the vacuum pump.
6. Open the vacuum pump valve #1.
7. Open the gas tank valve #2. The system will now evacuate the manifold and the lines. Wait several minutes to give the system time to evacuate. The sound of some mechanical pumps will change when they have evacuated the lines.
8. Open the gas fill valve #5 and wait several minutes for the system to evacuate the regulator.
9. Slowly open the gauge valve #3. Keep pumping until the gauge reads 0.
10. When the system is pumped down, close the filling gas valve #2 and open the tank valves #5 and #6. This will pressurize the regulator and lines with only filling gas.
11. Slowly open the LET detector valve #4. This will evacuate the detector. Wait until the gauge reads zero before proceeding to the filling phase.

Filling the Detector

Once the system has been evacuated you can fill the detector. Valves 1, 3, 4, 5, and 6 should be open and the system evacuated. Also the regulator should have been evacuated and filled with gas. If you performed the previous steps under Startup/evacuation then you have already performed these steps.

1. Close valve #1.
2. Slowly open valve #2 and fill the system to approximately 200 mmHg.
3. Close valve #2.

4. Open valve #1 and allow the gas to be vacuumed out of the entire system. Allow the needle to be between 0.25 and 0 mmHg before moving to the next step.
5. Repeat steps 1, 2, 3, and 4 five times to ensure all impurities are removed from the system.
6. Close valve #1.
7. Slowly open valve #2 and fill the system to approximately 56.3 mmHg.
8. Close valve #4.
9. Close valve #3.
10. Disconnect the hose from the ½ inch LET Detector.
11. Turn off the vacuum pump.
12. Ensure all valves are closed and fill gas is closed.
13. Detected is filled and ready to be used.

If you are going to use the LET Detector the next day it is recommended that you change out the gas in the GFS-1 daily. You should leave everything connected to the GFS-1 and under the condition when the LET Detector was disconnected to allow faster detector filling the next day.

Next Day Fill Procedures

1. Connect the LET Detector back into the GFS-1 as shown in Figure XX.
2. Ensure all valves are closed.
3. Open valves #5 and #6.
4. Open valves #3 and #4.
5. Turn on the vacuum pump.
6. Open valve #1 and allow the gas to be vacuumed out of the entire system. Allow the needle to be between 0.25 and 0 mmHg before moving to the next step.
7. Close valve #1.
8. Slowly open valve #2 and fill the system to approximately 200 mmHg.
9. Close valve #2.
10. Open valve #1 and allow the gas to be vacuumed out of the entire system. Allow the needle to be between 0.25 and 0 mmHg before moving to the next step.
11. Repeat steps 7, 8, 9, and 10 five times to ensure all impurities are removed from the system.
12. Close valve #1.
13. Slowly open valve #2 and fill the system to approximately 56.3 mmHg.
14. Close valve #4.
15. Close valve #3.
16. Disconnect the hose from the ½ inch LET Detector.
17. Turn off the vacuum pump.
18. Ensure all valves are closed and fill gas is closed.
19. Detected is filled and ready to be used.

APPENDIX C – TEPC

Appendix C gives results from 18, 19, and 20 December for TEPC experiments.

Following each figure is the tabulated data for the preceding plot.

Results from TEPC experiment on 18 December 2012

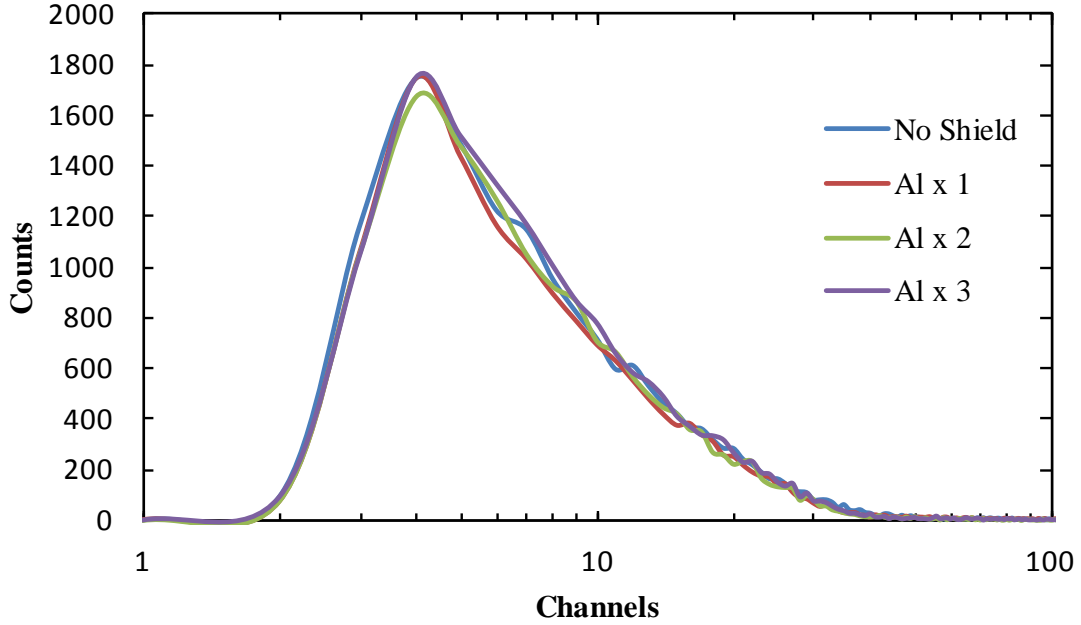


Figure 33: No shielding versus layers of aluminum on 18 December. The blue line is the result from no shielding, the red line is the result with one layer of aluminum shielding, the green line is the result of two layers of shielding, and the purple line is the result of three layers of shielding.

Table 15: No shielding versus layers of aluminum on 18 December.

Material	Total Counts	Percent Change Versus No Shielding
No Shield	16183 +/- 127.21	
Al x 1	14981 +/- 122.40	7.43 +/- 1.05
Al x 2	15347 +/- 123.88	5.17 +/- 1.07
Al x 3	16189 +/- 127.24	-0.04 +/- 1.11

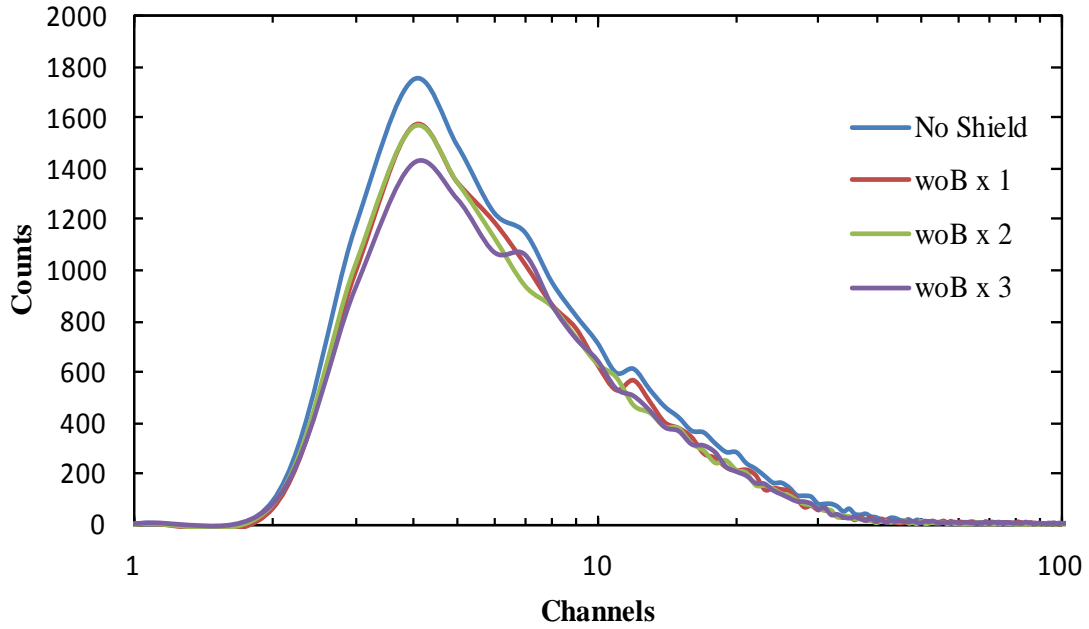


Figure 34: No shielding versus layers of sample X_{woB} on 18 December. The blue line is the result from no shielding, the purple line is the result with three layers of sample X_{woB} shielding, the green line is the result of two layers of sample X_{woB} shielding, and the red line is the results of one layer of sample X_{woB} shielding.

Table 16: No shielding versus layers of sample X_{woB} on 18 December.

Material	Total Counts	Percent Change Versus No Shielding
No Shield	16183 +/- 127.21	
woB x 1	14015 +/- 188.38	13.40 +/- 1.00
woB x 2	13758 +/- 117.29	14.98 +/- 0.99
woB x 3	13478 +/- 116.09	16.72 +/- 0.97

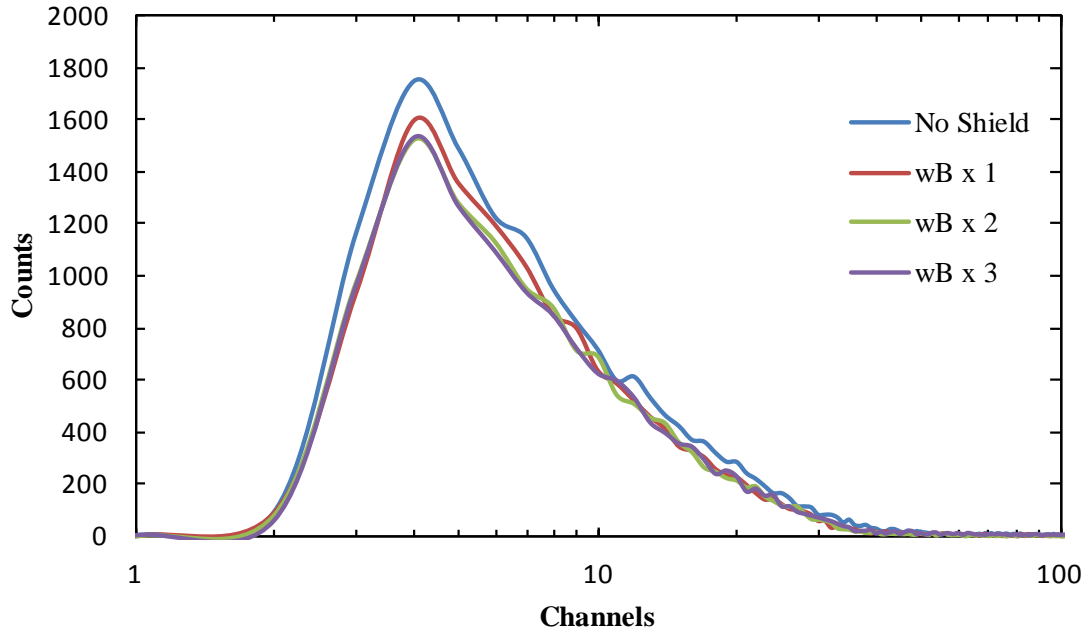


Figure 35: No shielding versus layers of sample X_{wB} on 18 December. The blue line is the result from no shielding, the purple line is the result with three layer of sample X_{wB} shielding, the green line is the result of two layer of sample X_{wB} shielding, and the red line is the result of one layer of sample X_{wB} shielding.

Table 17: No shielding versus layers of sample X_{wB} on 18 December.

Material	Total Counts	Percent Change Versus No Shielding
No Shield	16183 +/- 127.21	
wB x 1	14149 +/- 118.95	12.57 +/- 1.01
wB x 2	13785 +/- 117.41	14.82 +/- 0.99
wB x 3	13614 +/- 116.98	15.87 +/- 0.98

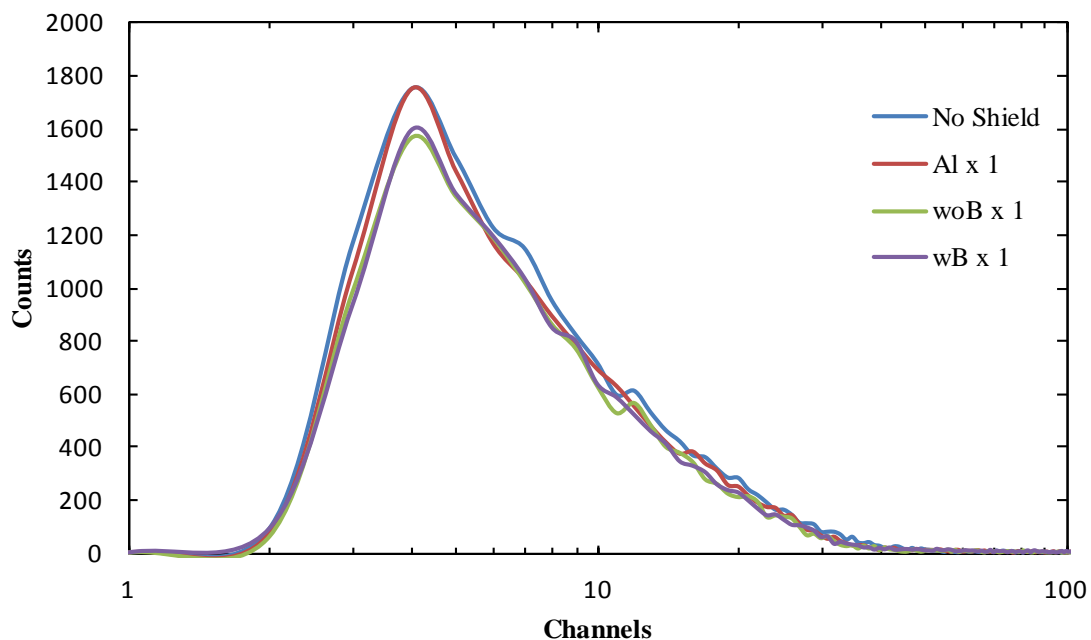


Figure 36: No shielding versus one layer of shielding material on 18 December. The blue line is the result from no shielding, the purple line is the result with one layer of sample X_{wB} shielding, the green line is the result with one layer of sample X_{woB} shielding, and red line is the result of one layer of T6061 shielding..

Table 18: No shielding versus one layer of shielding material on 18 December.

Material	Total Counts	Percentage Change Versus No shielding	Percent Change Versus Al x 1	Correcting for Density and Thickness Versus Al x 1
No Shield	16183 +/- 127.21			
Al x 1	14981 +/- 122.39	7.43 +/- 1.05		
woB x 1	14015 +/- 118.38	13.40 +/- 1.00	6.45 +/- 1.10	49.98 +/- 0.71
wB x 1	14149 +/- 118.95	12.57 +/- 1.01	5.55 +/- 1.11	20.11 +/- 0.98

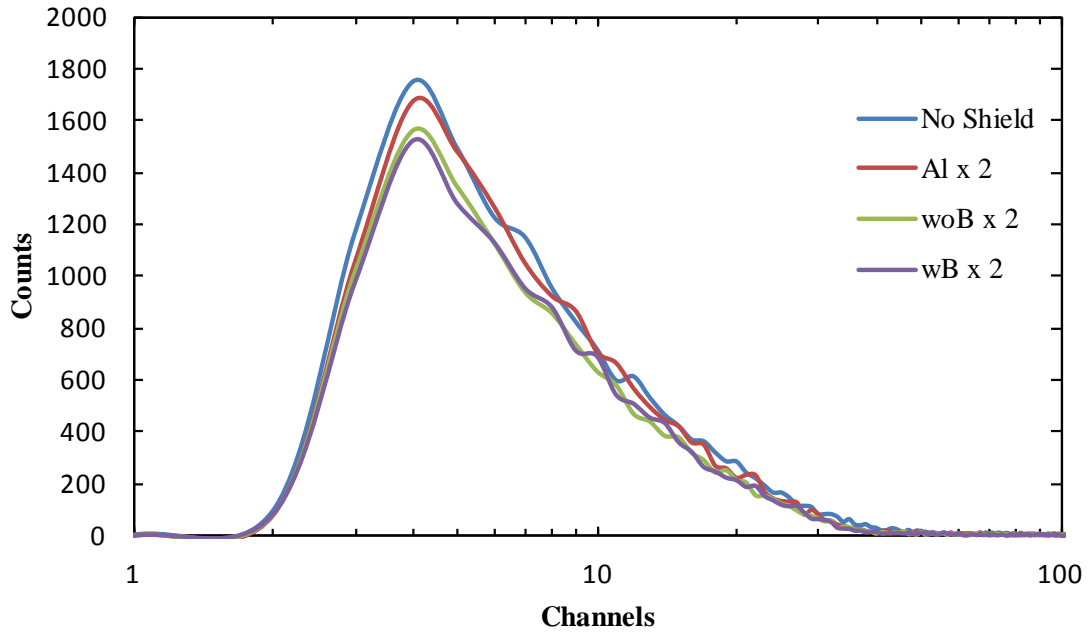


Figure 37: No shielding versus two layers of shielding material on 18 December. The blue line is the result from no shielding, the purple line is the result with two layers of sample X_{wB} shielding, the green line is the result with two layers of sample X_{woB} shielding, and red line is the result of two layers of T6061 shielding.

Table 19: No shielding versus two layers of shielding material on 18 December.

Material	Total Counts	Percentage Change Versus No shielding	Percent Change Versus Al x 2	Correcting for Density and Thickness Versus Al x 2
No Shield	16183 +/- 127.21			
Al x 2	15347 +/- 123.88	5.17 +/- 1.07		
woB x 2	13758 +/- 117.29	14.98 +/- 0.99	10.35 +/- 1.05	52.07 +/- 0.68
wB x 2	13785 +/- 117.41	14.82 +/- 0.99	10.18 +/- 1.05	24.02 +/- 0.93

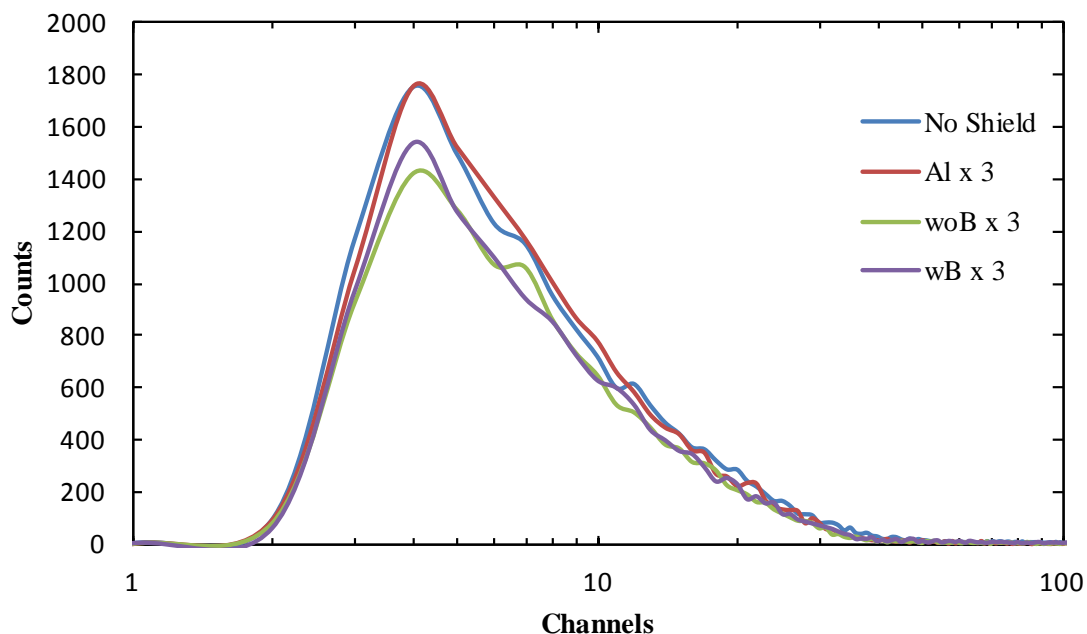


Figure 38: No shielding versus three layers of shielding material on 18 December. The blue line is the result from no shielding, the purple line is the result with three layers of sample X_{wB} shielding, the green line is the result with three layers of sample X_{woB} shielding, and red line is the result of three layers of T6061 shielding.

Table 20: No shielding versus three layers of shielding material on 18 December.

Material	Total Counts	Percentage Change Versus No shielding	Percent Change Versus Al x 3	Correcting for Density and Thickness Versus Al x 3
No Shield	16183 +/- 127.21			
Al x 3	16189 +/- 127.24	0.04 +/- 1.11		
woB x 3	13478 +/- 116.09	16.72 +/- 0.97	16.75 +/- 0.97	55.48 +/- 0.63
wB x 3	13614 +/- 116.68	15.87 +/- 0.98	15.91 +/- 0.98	28.87 +/- 0.87

Results of TEPC experiments on 19 December 2012

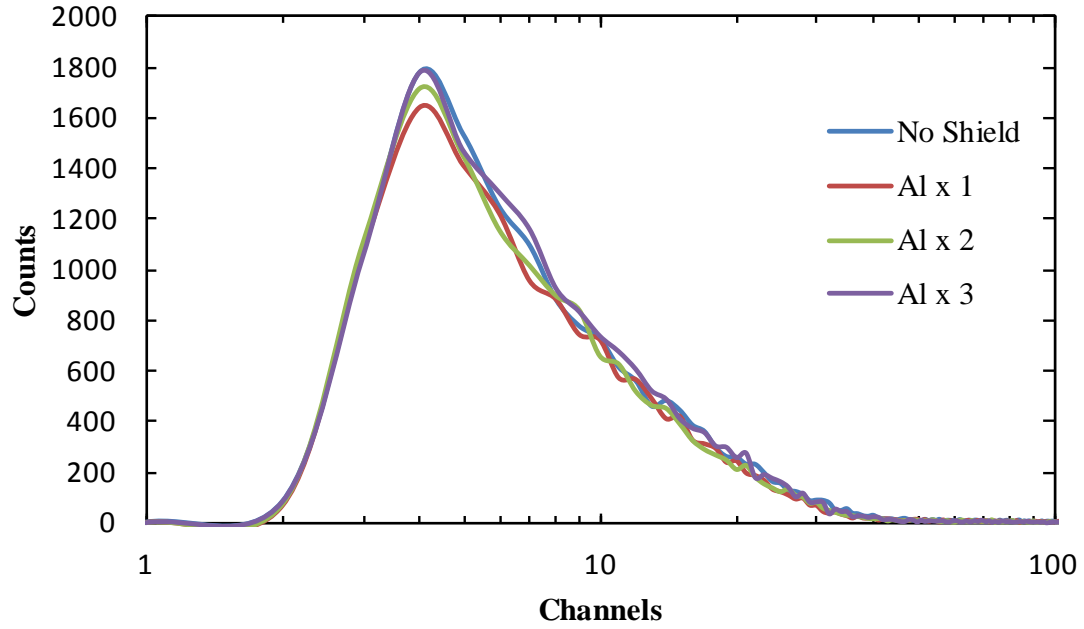


Figure 39: No shielding versus layers of aluminum on 19 December. The blue line is the result from no shielding, the red line is the result with one layer of aluminum shielding, the green line is the result of two layers of shielding, and the purple line is the result of three layers of shielding.

Table 21: No shielding versus layers of aluminum on 19 December.

Material	Total Counts	Percent Change Versus No Shielding
No Shield	15686 +/- 125.24	
Al x 1	14475 +/- 120.31	7.72 +/- 1.06
Al x 2	14746 +/- 121.43	5.99 +/- 1.08
Al x 3	15920 +/- 126.17	1.49 +/- 1.14

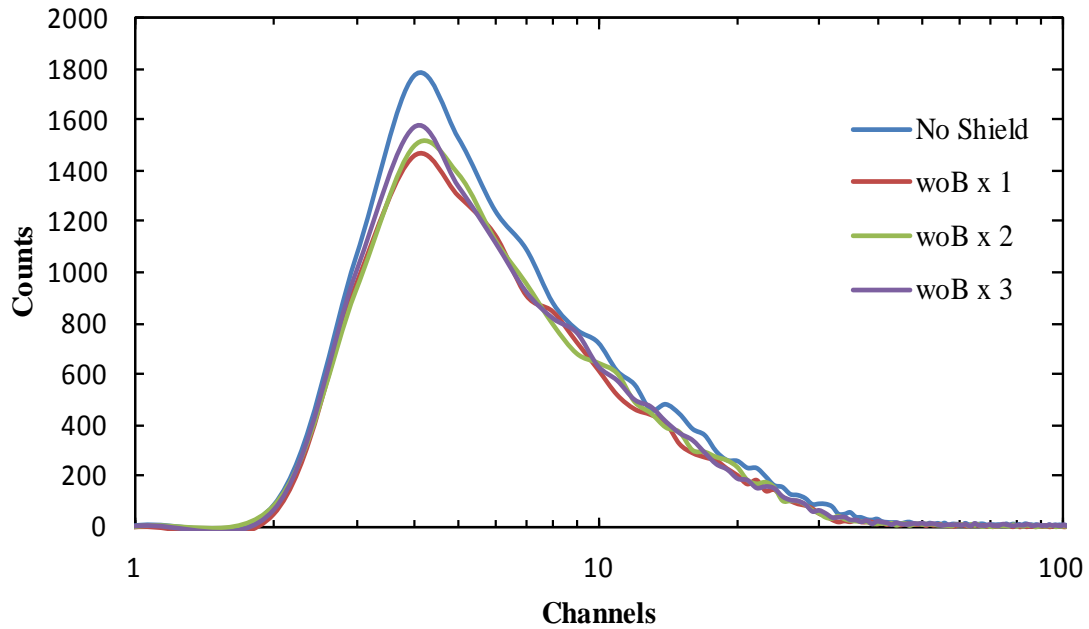


Figure 40: No shielding versus layers of sample X_{woB} on 19 December. The blue line is the result from no shielding, the purple line is the result with three layers of sample X_{woB} shielding, the green line is the result of two layers of sample X_{woB} shielding, and the red line is the result of one layer of sample X_{woB} shielding.

Table 22: No shielding versus layers of sample X_{woB} on 19 December.

Material	Total Counts	Percent Change Versus No Shielding
No Shield	15686 +/- 125.24	
woB x 1	13224 +/- 115.00	15.70 +/- 1.00
woB x 2	13637 +/- 116.78	13.06 +/- 1.02
woB x 3	13642 +/- 116.80	13.03 +/- 1.02

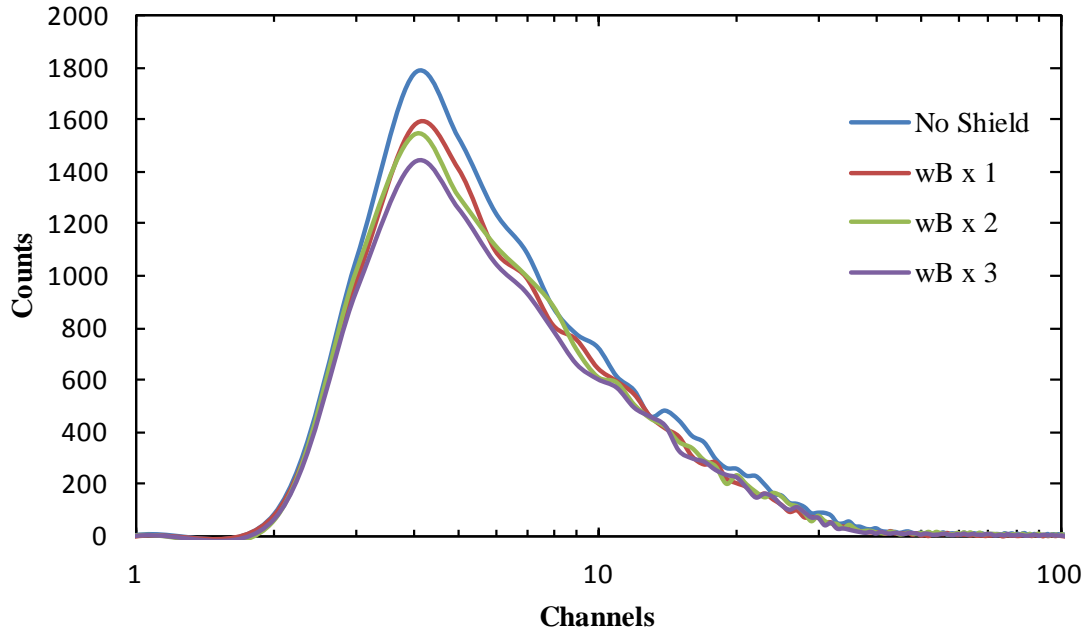


Figure 41: No shielding versus layers of sample X_{wB} on 19 December. The blue line is the result from no shielding, the purple line is the result with three layer of sample X_{wB} shielding, the green line is the result of two layer of sample X_{wB} shielding, and the red line is the result of one layer of sample X_{wB} shielding.

Table 23: No shielding versus layers of sample X_{wB} on 19 December.

Material	Total Counts	Percent Change Versus No Shielding
No Shield	15686 +/- 125.24	
wB x 1	14016 +/- 118.39	10.65 +/- 1.04
wB x 2	13924 +/- 118.00	11.23 +/- 1.03
wB x 3	13158 +/- 114.71	16.12 +/- 0.99

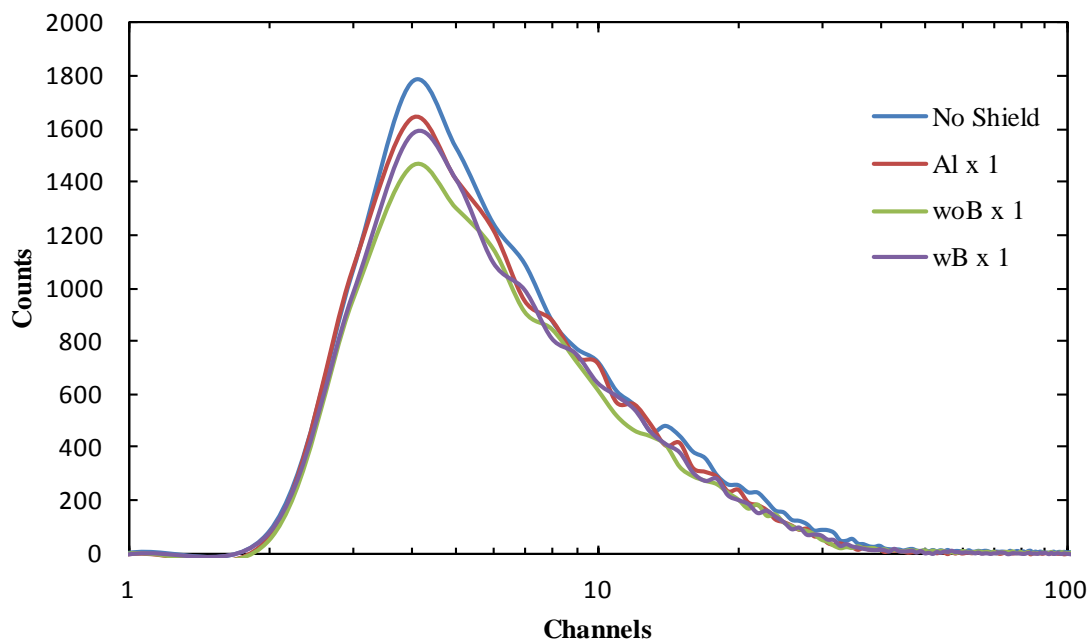


Figure 42: No shielding versus one layer of shielding material on 19 December. The blue line is the result from no shielding, the purple line is the result with one layer of sample X_{wB} shielding, the green line is the result with one layer of sample X_{woB} shielding, and red line is the result of one layer of T6061 shielding.

Table 24: No shielding versus one layer of shielding material on 19 December.

Material	Total Counts	Percentage Change Versus No shielding	Percent Change Versus Al x 1	Correcting for Density and Thickness Versus Al x 1
No Shield	15686 +/- 125.24			
Al x 1	14475 +/- 120.31	7.72 +/- 1.06		
woB x 1	13224 +/- 115.00	15.70 +/- 1.00	8.64 +/- 1.10	51.15 +/- 0.72
wB x 1	14016 +/- 118.39	10.65 +/- 1.04	3.17 +/- 1.15	18.10 +/- 1.01

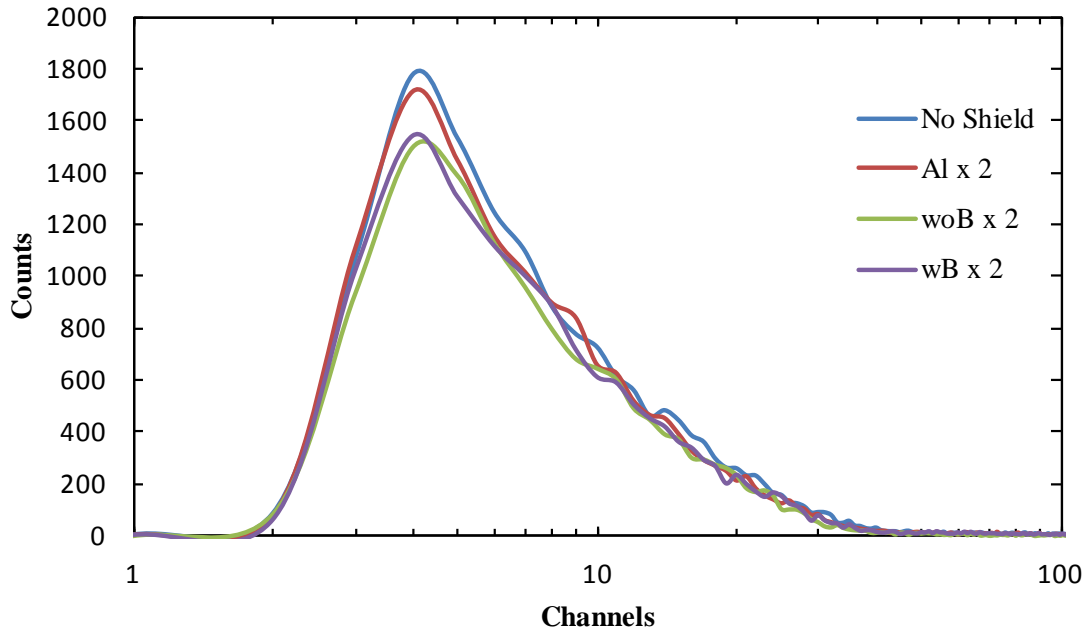


Figure 43: No shielding versus two layers of shielding material on 19 December. The blue line is the result from no shielding, the purple line is the result with two layers of sample X_{wB} shielding, the green line is the result with two layers of sample X_{woB} shielding, and red line is the result of two layers of T6061 shielding.

Table 25: No shielding versus two layers of shielding material on 19 December.

Material	Total Counts	Percentage Change Versus No shielding	Percent Change Versus Al x 2	Correcting for Density and Thickness Versus Al x 2
No Shield	15686 +/- 125.24			
Al x 2	14746 +/- 121.43	5.99 +/- 1.08		
woB x 2	13637 +/- 116.78	13.06 +/- 1.02	7.52 +/- 1.10	50.55 +/- 0.71
wB x 2	13924 +/- 118.00	11.23 +/- 1.03	5.57 +/- 1.12	20.13 +/- 0.99

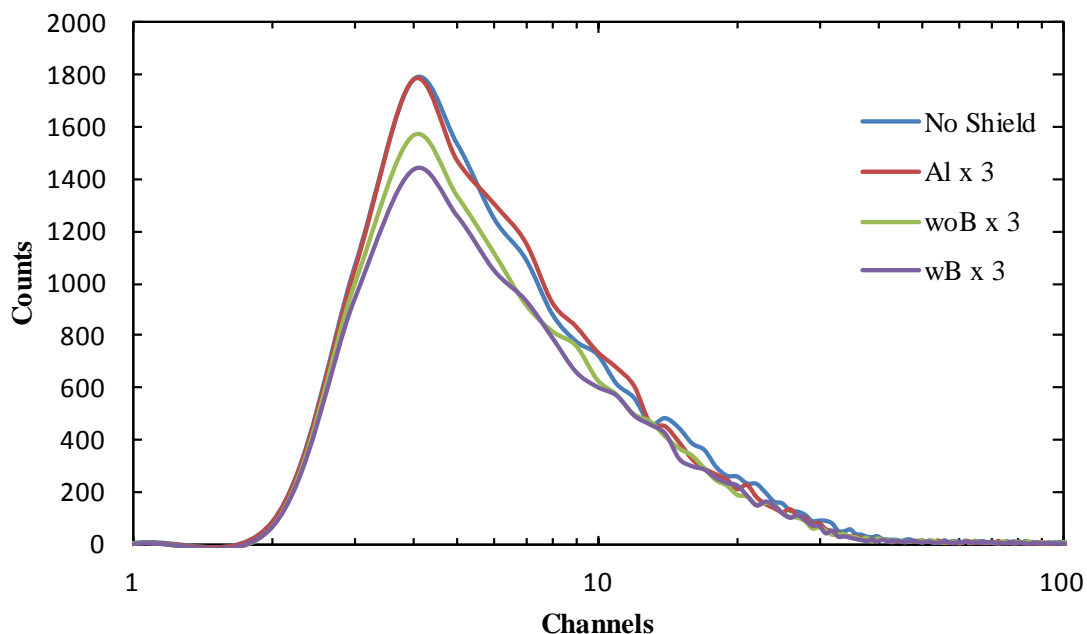


Figure 44: No shielding versus three layers of shielding material on 19 December. The blue line is the result from no shielding, the purple line is the result with three layers of sample X_{wB} shielding, the green line is the result with three layers of sample X_{woB} shielding, and red line is the result of three layers of T6061 shielding.

Table 26: No shielding versus three layers of shielding material on 19 December.

Material	Total Counts	Percentage Change Versus No shielding	Percent Change Versus Al x 3	Correcting for Density and Thickness Versus Al x 3
No Shield	15686 +/- 125.24			
Al x 3	15920 +/- 126.17	1.49 +/- 1.14		
woB x 3	13642 +/- 116.78	13.03 +/- 1.02	14.31 +/- 1.00	54.18 +/- 0.65
wB x 3	13158 +/- 114.71	16.12 +/- 0.99	17.35 +/- 0.97	30.09 +/- 0.86

Results of TEPC experiments on 20 December 2012

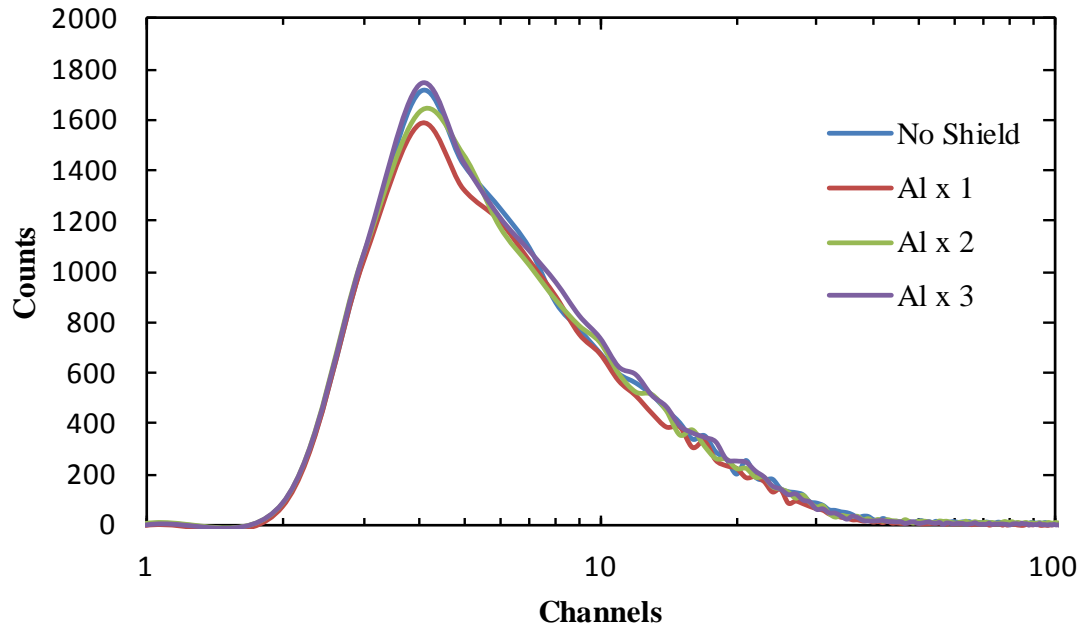


Figure 45: No shielding versus layers of aluminum on 20 December. The blue line is the result from no shielding, the red line is the result with one layer of aluminum shielding, the green line is the result of two layers of shielding, and the purple line is the result of three layers of shielding.

Table 27: No shielding versus layers of T6061 on 20 December.

Material	Total Counts	Percent Change Versus No Shielding
No Shield	15232 +/- 123.42	
Al x 1	14182 +/- 119.09	6.89 +/- 1.09
Al x 2	14643 +/- 121.01	3.87 +/- 1.11
Al x 3	15486 +/- 124.44	1.67 +/- 1.16

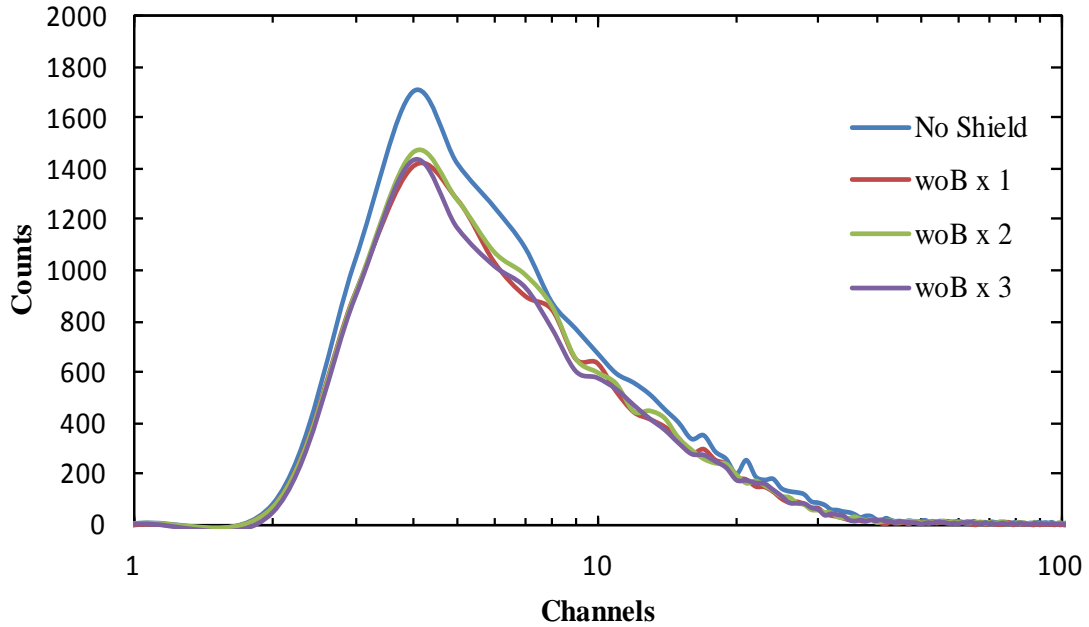


Figure 46: No shielding versus layers of sample X_{woB} on 20 December. The blue line is the result from no shielding, the purple line is the result with three layers of sample X_{woB} shielding, the green line is the result of two layers of sample X_{woB} shielding, and the red line is the result of one layer of sample X_{woB} shielding.

Table 28: No shielding versus layers of sample X_{woB} on 20 December.

Material	Total Counts	Percent Change Versus No Shielding
No Shield	15232 +/- 123.42	
woB x 1	12893 +/- 113.55	15.36 +/- 1.01
woB x 2	13050 +/- 114.24	14.33 +/- 1.02
woB x 3	12465 +/- 111.65	18.17 +/- 0.99

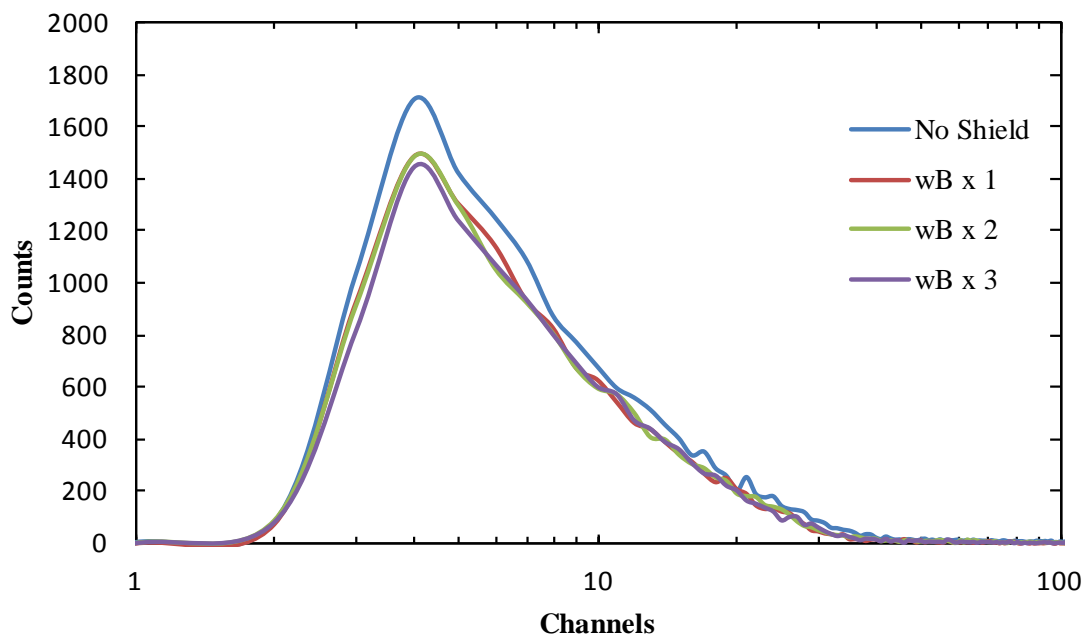


Figure 47: No shielding versus layers of sample X_{wB} on 20 December. The blue line is the result from no shielding, the purple line is the result with three layer of sample X_{wB} shielding, the green line is the result of two layer of sample X_{wB} shielding, and the red line is the result of one layer of sample X_{wB} shielding.

Table 29: No shielding versus layers of sample X_{wB} on 20 December.

Material	Total Counts	Percent Change Versus No Shielding
No Shield	15232 +/- 123.42	
wB x 1	13194 +/- 114.87	13.38 +/- 1.03
wB x 2	13170 +/- 114.76	13.54 +/- 1.03
wB x 3	12852 +/- 113.37	15.63 +/- 1.01

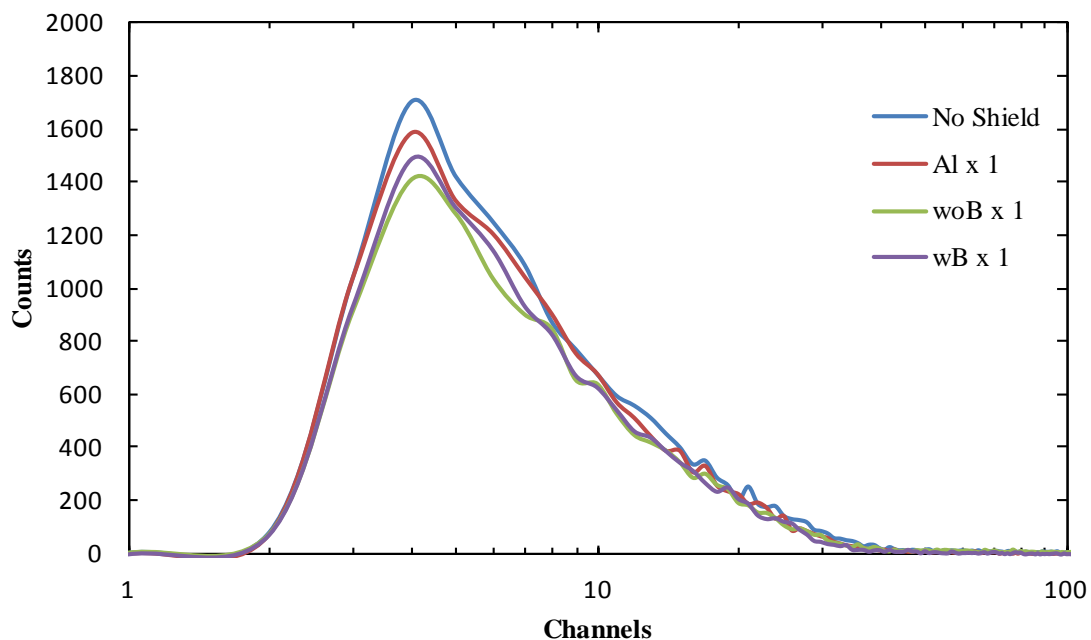


Figure 48: No shielding versus one layer of shielding material on 20 December. The blue line is the result from no shielding, the purple line is the result with one layer of sample X_{wB} shielding, the green line is the result with one layer of sample X_{woB} shielding, and red line is the result of one layer of T6061 shielding.

Table 30: No shielding versus one layer of shielding material on 20 December.

Material	Total Counts	Percentage Change Versus No shielding	Percent Change Versus Al x 1	Correcting for Density and Thickness Versus Al x 1
No Shield	15232 +/- 123.42			
Al x 1	14182 +/- 119.09	6.89 +/- 1.09		
woB x 1	12893 +/- 113.55	15.36 +/- 1.01	9.09 +/- 1.11	51.39 +/- 0.71
wB x 1	13194 +/- 114.87	13.38 +/- 1.03	6.97 +/- 1.13	21.31 +/- 1.00

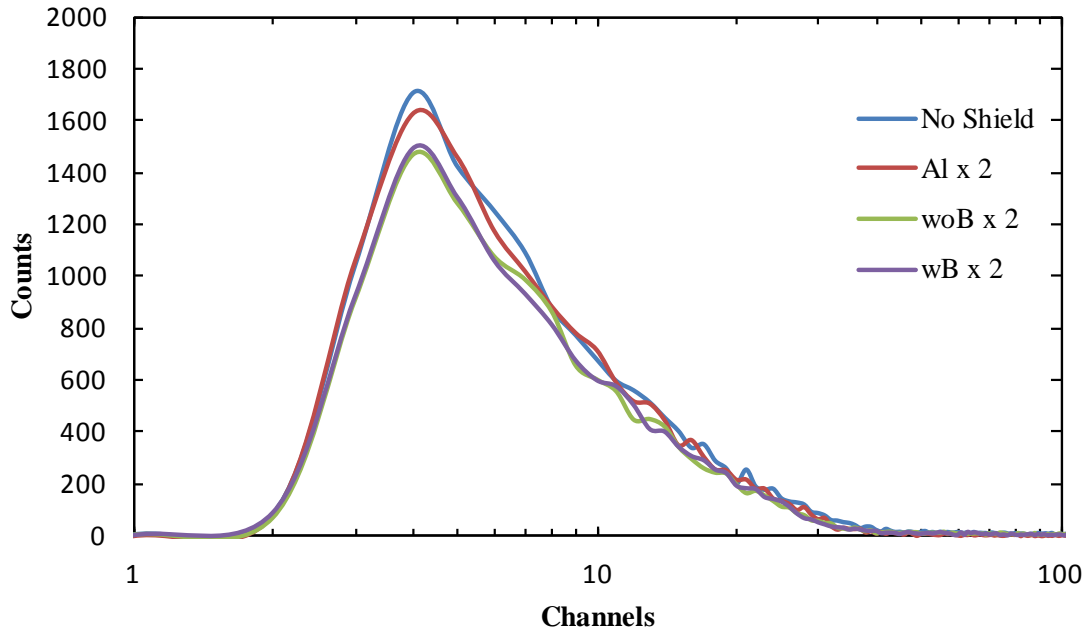


Figure 49: No shielding versus two layers of shielding material on 20 December. The blue line is the result from no shielding, the purple line is the result with two layers of sample X_{wB} shielding, the green line is the result with two layers of sample X_{woB} shielding, and red line is the result of two layers of T6061 shielding.

Table 31: No shielding versus two layers of shielding material on 20 December.

Material	Total Counts	Percentage Change Versus No shielding	Percent Change Versus Al x 2	Correcting for Density and Thickness Versus Al x 2
No Shield	15232 +/- 123.42			
Al x 2	14643 +/- 121.01	3.87 +/- 1.11		
woB x 2	13050 +/- 114.24	14.33 +/- 1.02	10.88 +/- 1.07	52.35 +/- 0.69
wB x 2	13170 +/- 114.76	13.54 +/- 1.03	10.06 +/- 1.08	23.92 +/- 0.96

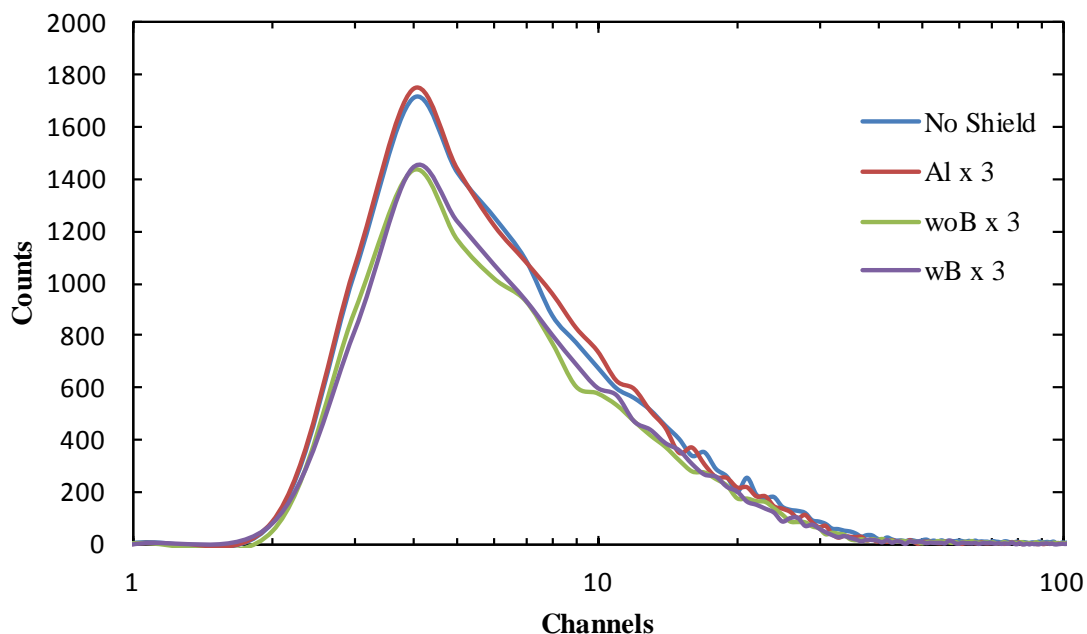


Figure 50: No shielding versus three layers of shielding material on 20 December. The blue line is the result from no shielding, the purple line is the result with three layers of sample X_{wB} shielding, the green line is the result with three layers of sample X_{woB} shielding, and red line is the result of three layers of T6061 shielding.

Table 32: No shielding versus three layers of shielding material on 20 December.

Material	Total Counts	Percentage Change Versus No shielding	Percent Change Versus Al x 3	Correcting for Density and Thickness Versus Al x 3
No Shield	15232 +/- 123.42			
Al x 3	15486 +/- 124.44	1.67 +/- 1.16		
woB x 3	12465 +/- 111.65	18.17 +/- 0.99	19.51 +/- 0.97	56.96 +/- 0.63
wB x 3	12852 +/- 113.37	15.63 +/- 1.01	17.01 +/- 0.99	29.80 +/- 0.88

APPENDIX D – Foil Activation

Appendix D gives results from the indium foil activation experiments when focusing on the thermal activation peaks of 1097 keV and 1294 keV.

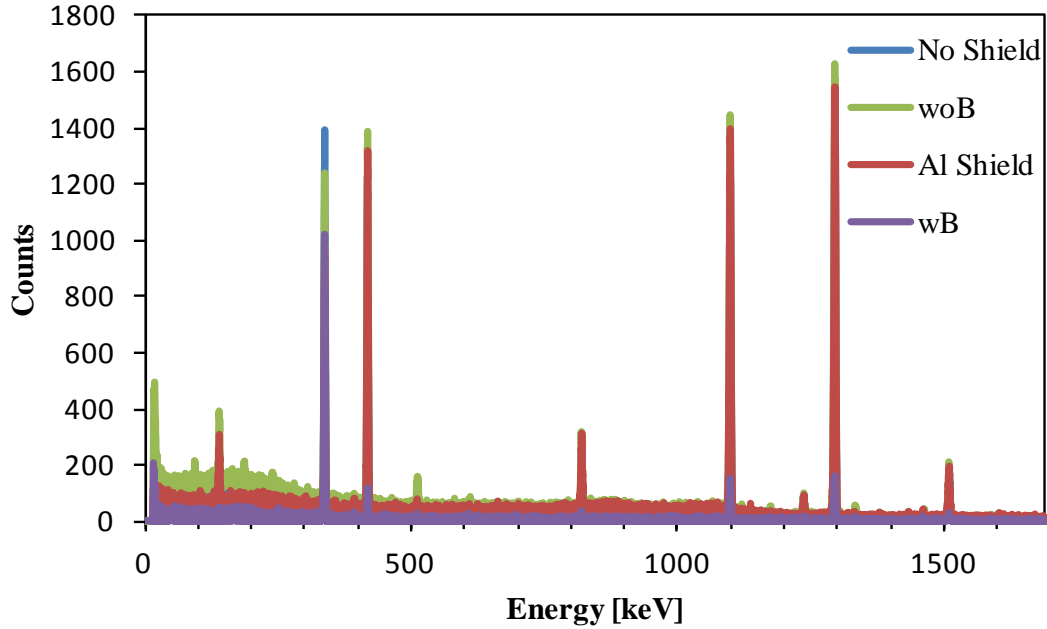


Figure 51: Foil activation spectrum of indium for thermal comparison after subtracting the background spectrum. This figure shows the results of four separate foil activation experiments. All experiments used the PuBe source to activate the indium foil. The blue spectrum is the result of the foil with no shielding. The green spectrum is the result of the foil with sample X_{woB} shielding. The purple spectrum is the result of the foil with sample X_{wB} . The red spectrum is the result of the foil with aluminum shielding.

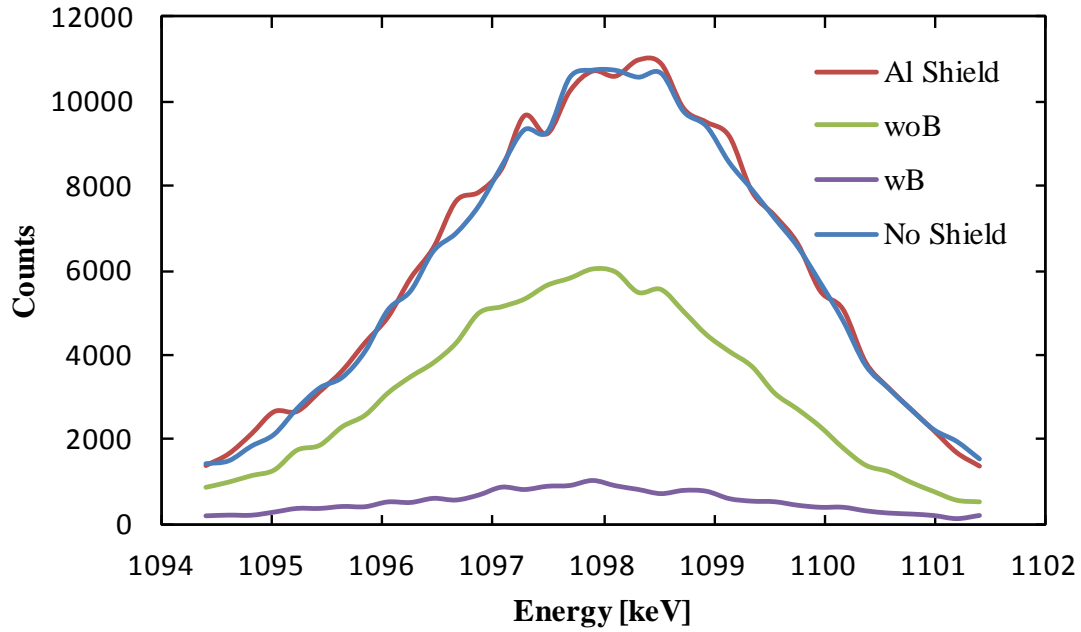


Figure 52: Foil activation spectrum of indium's 1097 keV peak corrected for weight, density, and thickness after subtracting the background spectrum. This figure shows the results of four separate foil activation experiments. All experiments used the Pu-Be source to activate the indium foil. The blue spectrum is the result of the foil with no shielding. The green spectrum is the result of the foil with sample X_{woB} shielding. The purple spectrum is the result of the foil with sample X_{wB} . The red spectrum is the result of the foil with aluminum shielding.

Table 33: Summary data for indium's 1097 keV peak after correcting for weight, density, and thickness

Percent Change against No Shielding				Percent Change against T6061 Shielding	
Material	Al Shield	woB Shield	wB Shield	woB Shield	wB Shield
Area	-1.46 +/- 2.20	46.91 +/- 1.20	91.50 +/- 0.27	47.67 +/- 1.85	91.62 +/- 0.39
Peak	-2.27 +/- 0.06	43.71 +/- 0.04	90.82 +/- 0.02	44.95 +/- 0.06	91.03 +/- 0.03

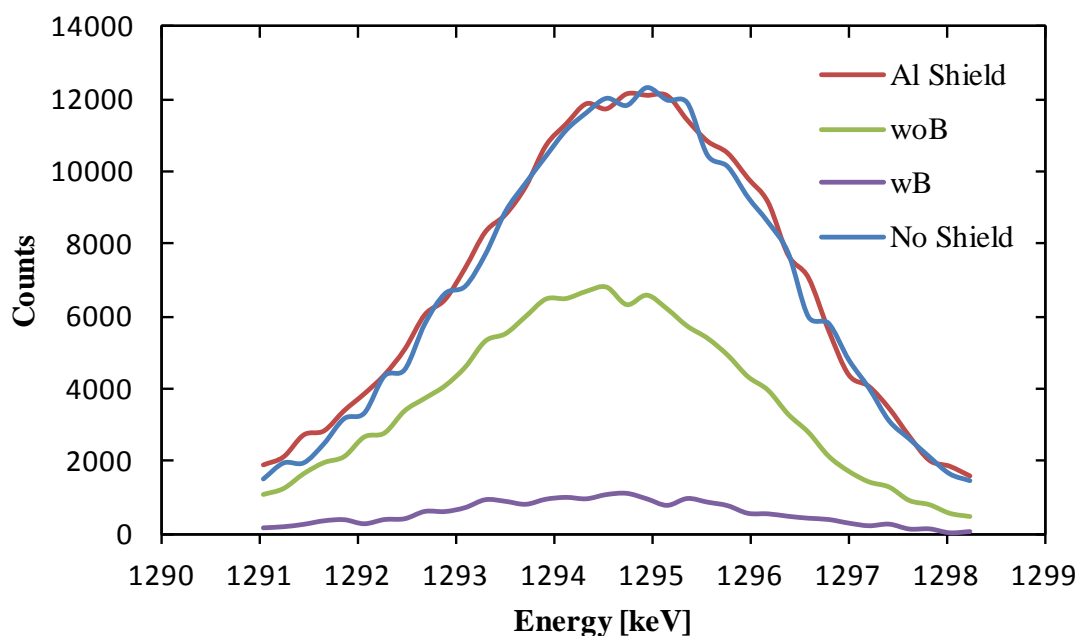


Figure 53: Foil activation spectrum of indium's 1294 keV corrected for weight, density, and thickness after subtracting the background spectrum. This figure shows the results of four separate foil activation experiments. All experiments used the Pu-Be source to activate the indium foil. The blue spectrum is the result of the foil with no shielding. The green spectrum is the result of the foil with sample X_{woB} shielding. The purple spectrum is the result of the foil with sample X_{wB} . The red spectrum is the result of the foil with aluminum shielding.

Table 34: Summary data for indium's 1294 keV peak after correcting for weight, density, and thickness

	Percent Change against No Shielding			Percent Change against T6061 Shielding	
	Al Shield	woB Shield	wB Shield	woB Shield	wB Shield
Area	-2.00 +/- 0.41	46.04 +/- 0.26	91.87 +/- 0.08	47.10 +/- 0.37	92.03 +/- 0.11
Peak	1.86 +/- 0.06	44.73 +/- 0.05	91.53 +/- 0.02	43.68 +/- 0.06	91.37 +/- 0.02

BIBLIOGRAPHY

- [1] L. F. Curtiss, *Introduction to Neutron Physics*. Princeton, New Jersey: Da Van Norstrand Company Inc., 1964.
- [2] J. Petrosky, "Radiation Effects on Electronic Devices, Modeling and Experiment,".
- [3] G. W. J. Swenson, "Looking back: Sputnik, The dawn of the space age," vol. 36, pp. 32-35, April 1994, .
- [4] K. S. Krane, *Introductory Nuclear Physics*. New York, NY: John Wiley and Sons Inc., 1987
- [5] G. F. Knoll, *Radiation Detection and Measurement*. New York: John Wiley and Sons, Inc, 2010.
- [6] Los Alamos National Security, LLC, Los Alamos National Laboratory., "Monte Carlo Code Group,".
- [7] Shultis, J.K. and Faw, R.E, "An MCNP Primer," 2 December 2011, .
- [8] ALCOA, "Alcoa Distribution and industrial Products, Understanding Extruded Aluminum Alloys," .
- [9] National Nuclear Data Center, "Evaluated Nuclear Data File (ENDF)".
- [10] J. S. Spears, "Characterizing a Neutron Energy Spectrum Using a “Forward Edge” Neutron Time-of-Flight Spectroscopy Technique," March 2005,
- [11] Technical Document Report No WADD-TR-61-174, Project No. 7001, Task No. 70012, "AF NETF Graphite Pile," March 1962 .
- [12] ORTEC, "Gamma Vision-32, Version 5.2, How to guide," .
- [13] Far West Technology, "LET Spectrum of ^{252}Cf ," .
- [14] Far West Technology, "Operation Manual for GFS-1," December 2001, .
- [15] Far West Technology, "Operation Manual for LET-1/2 detector," September 2008, .

REPORT DOCUMENTATION PAGE				Form Approved OMB No. 074-0188	
<p>The public reporting burden for this collection of information is estimated to average 1 hour per response, including the time for reviewing instructions, searching existing data sources, gathering and maintaining the data needed, and completing and reviewing the collection of information. Send comments regarding this burden estimate or any other aspect of the collection of information, including suggestions for reducing this burden to Department of Defense, Washington Headquarters Services, Directorate for Information Operations and Reports (0704-0188), 1215 Jefferson Davis Highway, Suite 1204, Arlington, VA 22202-4302. Respondents should be aware that notwithstanding any other provision of law, no person shall be subject to any penalty for failing to comply with a collection of information if it does not display a currently valid OMB control number.</p> <p>PLEASE DO NOT RETURN YOUR FORM TO THE ABOVE ADDRESS.</p>					
1. REPORT DATE (DD-MM-YYYY) 21 Mar 2013		2. REPORT TYPE Master's Thesis		3. DATES COVERED (From - To) 28 Jun 2010 - 21 Mar 2013	
4. TITLE AND SUBTITLE Neutron Shielding Effectiveness of Multifunctional Composite Materials				5a. CONTRACT NUMBER	
				5b. GRANT NUMBER	
				5c. PROGRAM ELEMENT NUMBER	
6. AUTHOR(S) Marchand, Anthony D., Major, USA				5d. PROJECT NUMBER	
				5e. TASK NUMBER	
				5f. WORK UNIT NUMBER	
7. PERFORMING ORGANIZATION NAMES(S) AND ADDRESS(S) Air Force Institute of Technology Graduate School of Engineering and Management (AFIT/ENV) 2950 Hobson Way, Building 640 WPAFB OH 45433-8865				8. PERFORMING ORGANIZATION REPORT NUMBER AFIT-ENP-13-M-25	
9. SPONSORING/MONITORING AGENCY NAME(S) AND ADDRESS(ES) Air Force Research Lab Max Alexander Jr. Program Lead, Electromagnetic Hardened Materials AFRL/RXBC 2941 Hobson Way Wright-Patterson AFB, OH 45433 (937) 255-9135				10. SPONSOR/MONITOR'S ACRONYM(S)	
				11. SPONSOR/MONITOR'S REPORT NUMBER(S)	
12. DISTRIBUTION/AVAILABILITY STATEMENT					
13. SUPPLEMENTARY NOTES					
14. ABSTRACT Composite materials offer a greater degree of flexibility in design and engineering of specialized space vehicle shielding applications compared to aluminum. A new design for shielding materials has been developed by including specific neutron absorbers and conductive materials into the composite structure. In this research, the neutron shielding capability of two types of custom-designed nanocomposite materials are compared to that of T6061 aluminum.					
15. SUBJECT TERMS Neutrons Shielding, Foil Activation, TEPC, MCNP					
16. SECURITY CLASSIFICATION OF:			17. LIMITATION OF ABSTRACT UU	18. NUMBER OF PAGES 104	19a. NAME OF RESPONSIBLE PERSON Dr. John W. McClory
a. REPORT U	b. ABSTRACT U	c. THIS PAGE U			19b. TELEPHONE NUMBER (Include area code) (937) 255-6565, x 7308 (john.mcclory@afit.edu)

Standard Form 298 (Rev. 8-98)
Prescribed by ANSI Std. Z39-18